



Improved Multi-Directional Forging Process and Its Effect on Microstructure and Three-Directional Mechanical Properties of 2195 Al-Li Alloy

Dengliang Tong^{1,2} · Youping Yi^{1,2} · Hailin He^{1,2} · Shiquan Huang^{1,2} · Jiaguo Tang³

Received: 30 March 2024 / Accepted: 26 May 2024

© The Author(s) under exclusive licence to The Korean Institute of Metals and Materials 2024

Abstract

Reticular crystal phases and abnormally coarse grains are key problems that restrict the improvement of the mechanical properties and uniformity of Al-Li alloys. The effects of the multidirectional forging (MDF) process on the microstructure at the edge and center and the three-directional mechanical properties of the 2195 Al-Li alloy were investigated. The results show that the strong deformation resistance produced by one heat forging at 400 °C with seven upsetting and six stretching (400-7U6S-1) fully broke the reticular crystal phases at the grain boundaries and obtained the dispersed phase structure. The high density of dislocations accumulated by strong deformation promoted the dissolution of the dispersed secondary phases, and the area fraction of the secondary phase particles at the edge and center decreased from 3.88% and 1.97–0.75% and 0.61%, respectively, which prevented the occurrence of intergranular fractures and dramatically improved the ductility. Meanwhile, the dissolution of the second phases enhanced the precipitation force of the T1 phases and inhibited the precipitation of δ' phases. Furthermore, the higher density of dislocations significantly increased the nucleation rate of dynamic recrystallization and eliminated the abnormally coarse grains, and thus acquired a uniform ultra-fined grain structure and the average grain diameter was reduced from 159 μm to 17 μm. The tensile strength, yield strength and elongation in the width direction increased to 592 MPa, 545 MPa and 8.0%, respectively, and increased by 7.2%, 7.2% and 90.5%, respectively. In particular, the maximum difference in the elongation of the forgings in the width direction decreased from 83.3 to 11.1%.

Keywords Al-Li alloy · Multidirectional forging process · Ultrafine grains · Reticular crystal phases · Three-directional mechanical properties

1 Introduction

Al-Li alloys not only have the advantages of low density, high elastic modulus and specific strength, but also have the characteristics of a low fatigue crack growth rate and excellent low temperature-performance, and are considered to be the most ideal structural materials in the aerospace field [1]. The 2195 Al-Li alloy is a third-generation Al-Li alloy mainly used in the manufacture of fuel tanks for launch vehicles [2]. Using the 2195 Al-Li alloy instead of the 2219 Al-Cu alloy to manufacture a launch vehicle fuel tank, the structural mass is reduced by 5%, the carrying capacity is increased by 3.4 t, and the cost is reduced by approximately 75 million US dollars [3]. Therefore, the development of high-performance Al-Li alloys is extremely significant in the aerospace field.

✉ Youping Yi
yyp@csu.edu.cn

✉ Hailin He
hehailin0621@126.com

¹ Light Alloy Research Institute, Central South University, Changsha 410083, China

² State Key Laboratory of Precision Manufacturing for Extreme Service Performance, Changsha 410083, China

³ School of Mechanical and Electrical Engineering, Central South University, Changsha 410083, China

Currently, the manufacturing methods for 2195 Al-Li alloy ingots mainly include casting,

spray deposition and powder metallurgy [4, 5]. Among them, casting is the most extensively used method for producing 2195 alloy ingots [6]. However, defects such as micro segregation inevitably form in the casting process owing to the uneven cooling rate, which is more serious in the casting process of large-scale ingots [7]. Relevant studies have shown that casting defects are mainly expressed as abundant residual crystal phases that segregate at the grain boundary and present a reticular distribution [8–10]. Moreover, these uneven crystal phases are inherited by the final heat-treated components [11], resulting in the initiation of cracks at the grain boundaries and a severe reduction in plasticity.

Severe plastic deformation (SPD) can improve the casting structure and distribution of residual crystal phases [12]. This method is effective in improving non-uniform casting defects and material properties [13]. Conventional methods of SPD include multidirectional forging (MDF) [14], equal channel angular pressing (ECAP) [15], high-pressure torsion (HPT) [16] and accumulative rolling (AR) [17]. Among these, the MDF process is widely used for the cogging of large ingots because it can prepare bulk materials without special and complex mold structures. During MDF, the forging temperature, degree of deformation and speed significantly affect the microstructural evolution and mechanical properties of the alloy [18, 19]. Zhang et al. prepared large-scale commercial AZ80 Mg alloy forgings using MDF and aging processes and found that the high density of dislocations and subgrain boundaries generated by MDF accelerated the aging response, and the formed bimodal microstructure and nanoscale precipitated phases improved the strength and plasticity of the alloy [20]. He et al. studied the effect of MDF temperature on the microstructure and mechanical properties of 2219 Al alloy, and found that increasing the MDF temperature can promote the dissolution of a large number of Al_2Cu particles and improve the mechanical properties of the forging. The optimal forging temperature of 2219 Al alloy is 510 °C [10]. Wang et al. reported that the large plastic deformation accumulated by MDF enhanced the texture and refined the grain structure of a Mg-Gd-Y-Zn-Zr-Ag alloy [21]. Wang et al. found that the coarse second-phase particles in 2A14 Al alloy gradually spheroidized during the process of MDF at 480 °C, which improved the uniformity of the three-dimensional mechanical properties of the alloy [22].

In addition, the grain structure can be refined and the strength and plasticity of the alloy can be improved by MDF. Anastasia V et al. found that during the process of MDF, the recrystallization nucleation induced by the β phase refined grains and increased the yield strength of the alloy [23].

Cui et al. proposed a small-strain MDF process with gradient cooling for the preparation of AZ31 Mg alloy forgings. When the cumulative strain reached 2.7, a uniform fine-grained structure and bimodal basal texture were obtained [24]. Sun et al. obtained ultrafine grains using MDF and improved the yield strength of 304 L stainless steel [25]. Paula et al. studied the effect of cumulative strain during MDF on the thermal stability of copper alloys and found that with an increase in cumulative strain, the thermal stability related to static recrystallization gradually decreased, and finer grain structures were obtained [26].

Nevertheless, there are only a few studies on the influence of upsetting and stretching methods on the microstructure of the edge and center and the three-directional mechanical properties of the 2195 Al-Li alloy. In this study, the effects of four types of MDF processes on the microstructural uniformity and mechanical properties of 2195 Al-Li alloys were systematically studied. A new MDF process that fully disperses the residual crystal phases and refines the grains of the 2195 Al-Li alloy was proposed. In summary, these research results provide theoretical and technical references for the development of high-performance Al-Li alloy forgings for aerospace applications.

2 Experimental Procedure

The experimental material used in this study was a large-scale 2195 Al-Li alloy ingot cast by the Light Alloy Research Institute of Central South University. The chemical composition of the ingot was as follows: Al–4.25%Cu–1.13%Li–0.39%Mg–0.45%Ag–0.12%Fe–0.11%Zr–0.04%Mn (wt). First, a cylindrical sample with a thickness of 200 mm was cut from the large 2195 Al-Li alloy ingot (\varnothing 400 mm \times 1000 mm) after homogenization. Subsequently, four quarter ingots (190 mm \times 190 mm \times 200 mm) were cut along the diameter of the cylindrical sample. A sampling diagram is shown in Fig. 1. The four samples were forged using different MDF processes on a 40 MN numerically-controlled hydraulic press at a forging speed of 10 mm/s. Figure 2 shows the principle of MDF (in each step, the black and purple lines represent the contours of the sample before and after forging, respectively). Before the MDF, the mold was heated to 470 °C at a rate of 5 °C/min and held for 2 h to ensure heat penetration, while the specimen was heated to 400 °C and 480 °C at the same speed and held for 2 h. MoS_2 was used as a lubricant at the interface between the die and specimen to achieve homogeneous deformation. During the MDF process, the ingot was stretched axially to prepare a rectangular specimen, and then separately upset (the specimen was compressed along different axial directions with a height reduction of 60%) and stretched (the specimen

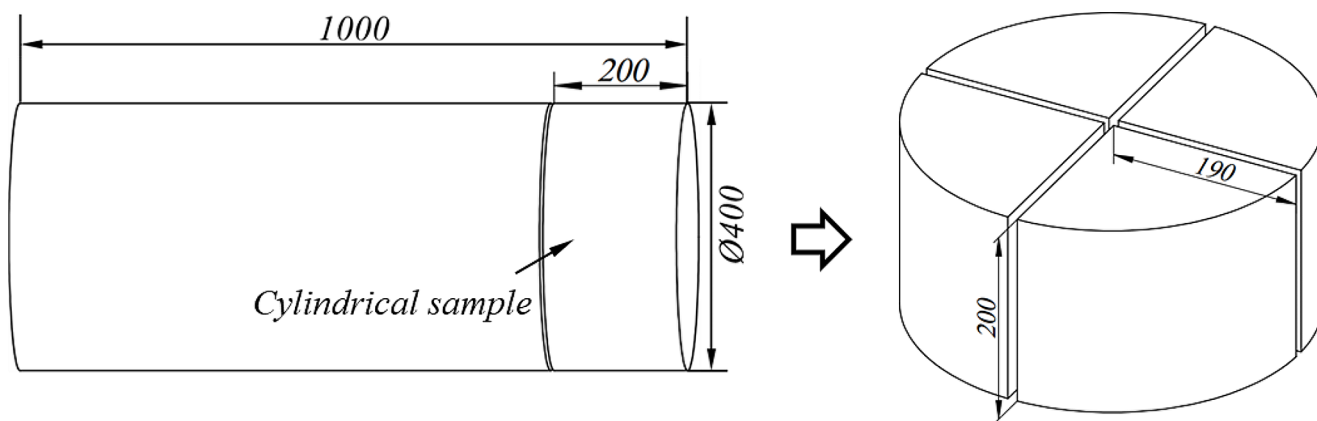


Fig. 1 Sketch of sampling from large ingot (dimensions are in mm)

was compressed in two specified directions so that it was stretched in the undeformed direction). The four MDF processes differed in the number of upsets and stretches, forging temperature and heating number. Figure 2 (a) shows the four-upsetting and three-stretching MDF process, designated as 4U3S. As shown in Fig. 2 (b), the seven upsetting and six stretching process (7U6S) were achieved by repeating the 4U3S process. The MDF processes of 4U3S and 7U6S accumulated strains of 1.8 and 3.6, respectively. The names of the different processes are shown in Table 1. During twice-heating forging, the annealing time was 2 h. After MDF, the sample was annealed for 2 h at 480 °C at a heating rate of 5 °C/min and then forged at 480 °C with a deformation of 40%. The air-cooled sample was subjected to solution treatment at 500 °C for 4 h and quenched in water at room temperature. After cold deformation in the height direction with a deformation of 3% at room temperature, the sample was immediately artificially aged at 160 °C for 24 h and then air-cooled. Research results showed that 2195 Al-Li alloy maintained a high elongation while the strength did not decrease after aging at 160 °C for 24 h [27]. Therefore, the aging temperature of 160 °C was selected. The process route is illustrated in Fig. 3.

The microstructures of the samples after homogenization, MDF, annealing, and T8 heat treatment (solution treatment + cold deformation + artificial aging) were analyzed to study the microstructural evolution of the 2195 Al-Li alloy during deformation and treatment. To detect the homogeneity of the mechanical properties of the alloy, tensile samples at the edge, quarter and center positions of the forgings in the three directions of length, width and height were taken for mechanical property testing. A sampling diagram and the tensile specimens are shown in Fig. 4. A tensile testing machine (CMT5105GL) was used to test the mechanical properties of the Al-Li alloy after heat treatment at a tensile speed of 2 mm/min. The influence of the MDF process on the microstructure uniformity of 2195 Al-Li alloy was

analyzed, and the microstructure at the edge and center of the samples after MDF and heat treatment was observed, as well as the transverse and longitudinal microstructures at each position after heat treatment (as shown in Fig. 4). The EBSD samples were prepared by electropolishing at -25 – -30 °C for a mixture of 30% nitric acid and 70% ethanol. Scanning electron microscopy (SEM, TESCAN-MIRA3LMU) was used to observe the distribution of the secondary phase particles and the characteristics of the fracture surfaces. The heat-treated samples were ground and etched using Keller's reagent, and an optical microscope (OM, OLYMPUS DSX500) to observe the grain structure of the alloy. The samples were ground to 50–80 μm, punched to Ø3 mm disks, and thinned using a double jet instrument (Tenupol-5). Transmission electron microscopy (TEM, Talos F200) was used to observe the dislocation configurations, substructures and precipitated phases of the alloys.

3 Results

3.1 Initial Microstructures

Figure 5 shows the SEM images of large-scale 2195 Al-Li alloy ingot after homogenization. It can be observed that abundant crystal phases formed in the casting process were unevenly distributed. These coarse crystal phases precipitated continuously along the grain boundaries and form a reticular structure, which deteriorated the mechanical properties of the alloy. Additionally, numerous needle-like phases were observed, which were secondary phases that precipitated from the matrix with decreasing temperature. The crystal phases at the grain boundaries detected by Energy Dispersive Spectroscopy (EDS) were the Al-Cu phase, and the intracrystalline needle-like phases were identified as containing Cu and Ag phases (Fig. 5 (c, d)).

Fig. 2 Schematic of multidirectional forging process

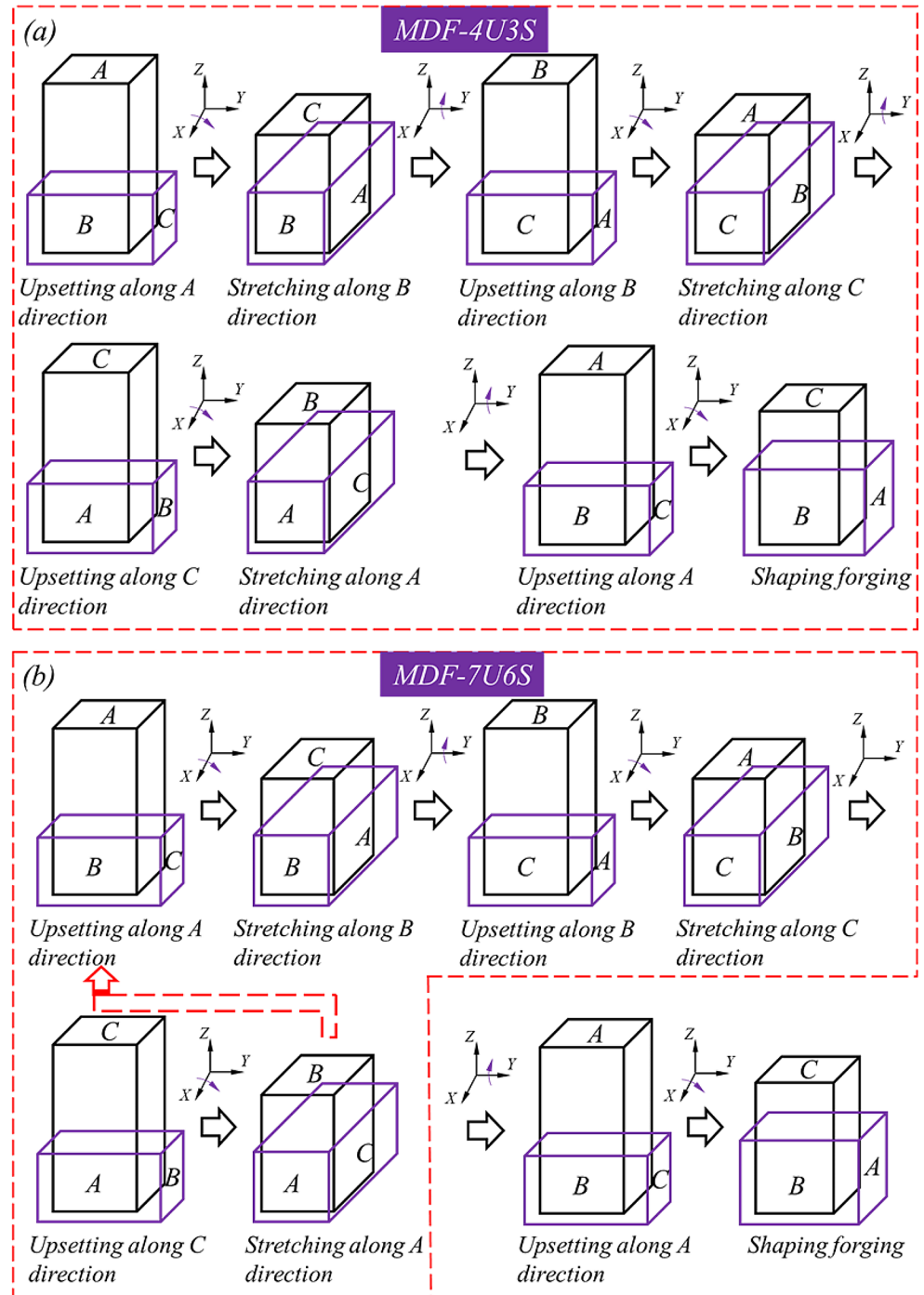


Table 1 Designation of different MDF processes

Process	Forging temperature	MDF method	Heating number
400-4U3S-1	400 °C	Four-upsetting and three-stretching	1
480-7U6S-2	480 °C	Seven-upsetting and six-stretching	2
480-7U6S-1	480 °C	Seven-upsetting and six-stretching	1
400-7U6S-1	400 °C	Seven-upsetting and six-stretching	1

According to Zhang et al., the coarse crystal phase at the grain boundaries was Al_2Cu [8].

Figure 6 shows the EBSD image of large-scale 2195 Al-Li alloy ingot after homogenization. The initial grains of the ingot were coarse and uneven, with an average grain diameter of 212 μm . The orientation difference of adjacent grains was greater than 15° , and the grain boundaries were high-angle grain boundaries (HAGBs).

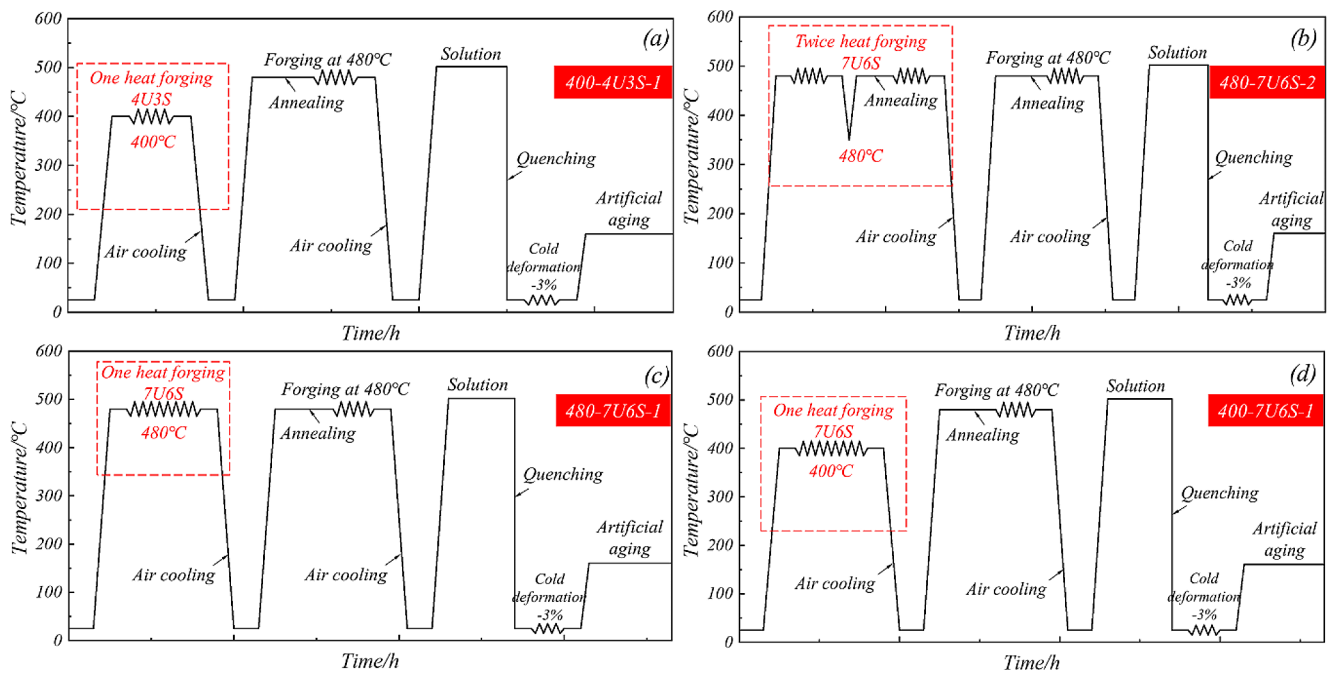


Fig. 3 Schematic of the four MDF processing routes

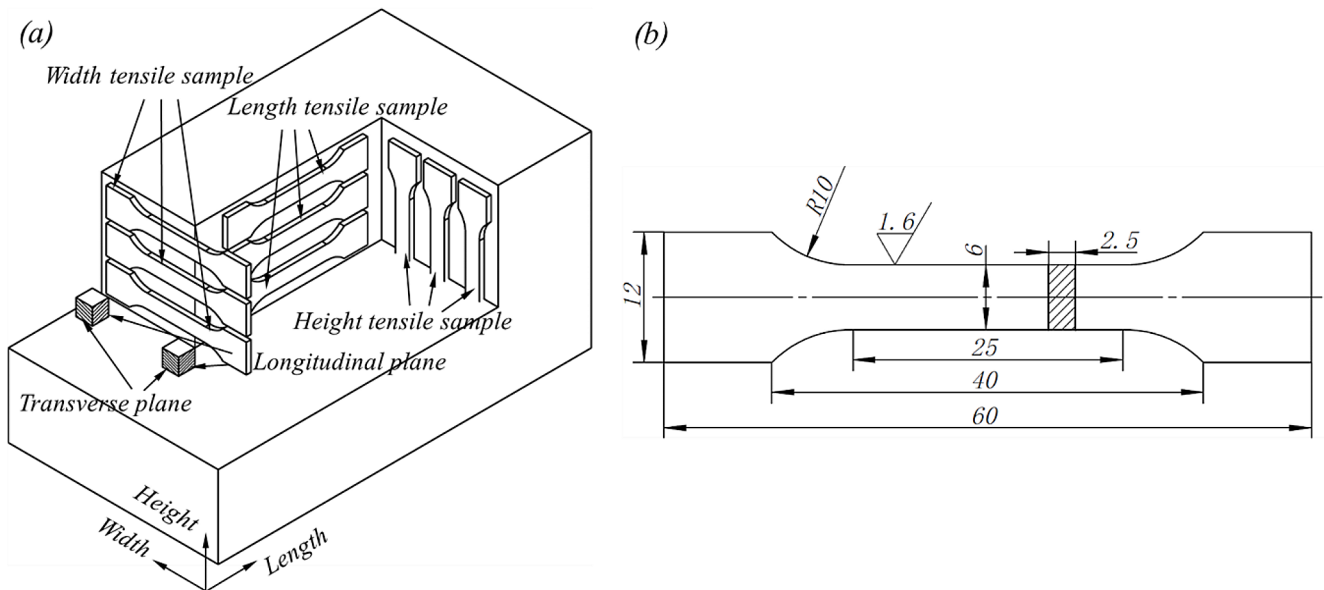


Fig. 4 Schematic of sampling: (a) cutting samples for tensile testing and microstructure observation and (b) schematic of the tensile specimens (dimensions are in mm, R: transitional arc radius)

3.2 Microstructures after MDF and Annealing

3.2.1 Evolution of Crystal Phases

The abundant coarse reticular crystal phases distributed along the grain boundaries in the 2195 Al-Li alloy ingots have an important effect on the mechanical properties. Therefore, the effects of the MDF processes on the coarse crystal phases and microstructure uniformity were studied.

Figure 7 shows the SEM images of the edge and center of the 2195 Al-Li alloy after different MDF processes. It can be seen that the coarse crystal phases have a certain degree of fragmentation after MDF. After adopting the MDF process for 400-4U3S-1, the distribution of the crystal phases was the worst, similar to that of the casting structure. A large number of crystal-phase particles at the edge and center were still accumulated around the grain boundaries (Fig. 7 (a1–a4)). The crystal-phase particles at the edge

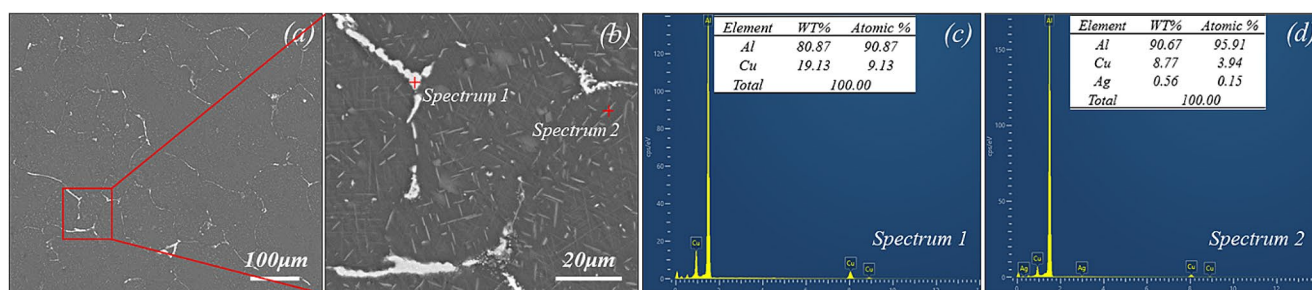


Fig. 5 SEM images of the as-homogenized ingot: (a) low-magnification SEM image; (b) high-magnification SEM image; (c, d) EDS analysis results

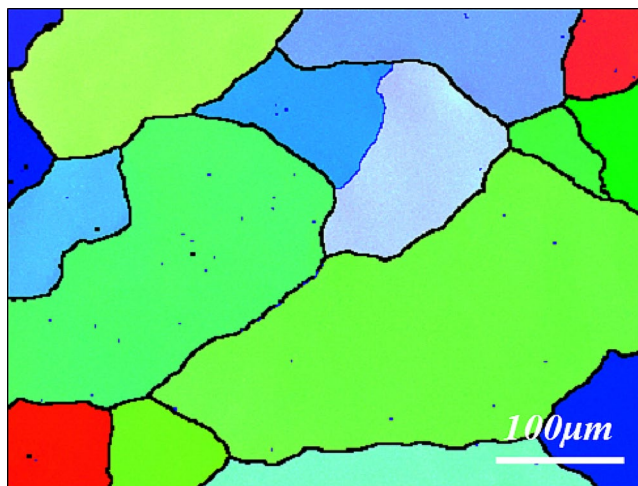


Fig. 6 EBSD images of the as-homogenized ingot

of the sample obtained using the 480-7U6S-2 process still exhibited a reticular distribution, but the degree of aggregation was weakened (Fig. 7 (b1, b2)). The crystal phases at the central position presented a striped distribution along the flow direction (Fig. 7 (b3, b4)). When the intermediate annealing process was stopped and the 480-7U6S-1 process was adopted, the reticular structure of the crystal phases at the edge of the sample disappeared; however, particle aggregation was observed. At the central position, abundant crystal phases tended to disperse, and no crystal phase aggregation was observed (Fig. 7 (c1–c4)). After the MDF process of 400-7U6S-1, the crystal phase particles at the edge and center of the samples were evenly distributed and dispersed, and no reticular crystal phase aggregation was observed (Fig. 7 (d1–d4)).

3.2.2 Evolution of Grain Structure

Figure 8 shows EBSD images of the edge and center of the 2195 Al-Li alloy after different MDF processes. In the figure, the black line represents HAGBs with a difference in orientation greater than 15° , and the red line represents low-angle grain boundaries (LAGBs) with a difference in

orientation between 2° and 15° . Compared with the as-cast grains, the grain diameter after MDF was significantly reduced, indicating that dynamic recrystallization occurred during the MDF process. The dynamic recrystallization of the samples with the 480-7U6S-2 and 480-7U6S-1 processes was low at the edge and center, and only a small number of HAGBs were observed, as shown in Fig. 9. However, the HAGBs ratio of 480-7U6S-1 samples was higher than that of 480-7U6S-2 samples. After adopting the MDF process of 400-4U3S-1, the proportion of HAGBs at the edge and the center of the sample increased to 16% and 34%, respectively (Fig. 10), indicating that the degree of dynamic recrystallization increased, and the recrystallization degree at the center was higher than that at the edge. However, the degree of recrystallization at local locations was low and a few coarse grains were observed. We found that the proportion of HAGBs at the edge and center of the sample after MDF of the 400-7U6S-1 process increased to 43% and 37%, respectively, indicating that the degree of recrystallization was significantly improved. In addition, the grains at the edge and center of the samples were equiaxed and fine grains with average sizes of $8 \mu\text{m}$ and $15 \mu\text{m}$, respectively. Notably, no coarse grains were observed at the edge and the center (Fig. 9 (d1, d2)). It can be seen that the degree of dynamic recrystallization degree and grain uniformity were significantly improved by MDF at 400°C and by increasing the number of upsetting and stretching.

To figure out whether the equiaxed and fine grains obtained after MDF grew during subsequent annealing, the EBSD image of the center position of the 2195 Al-Li alloy after annealing was obtained (Fig. 11). It can be observed that the grains after annealing do not grow significantly, which was similar to the grain structure after MDF. This indicated that no significant static recrystallization occurred during annealing. After annealing, coarse grains with a size of $\sim 80\text{--}120 \mu\text{m}$ still exist in the samples adopting the MDF process of 400-4U3S-1, 480-7U6S-2 and 480-7U6S-1. Annealed samples adopting the 400-7U6S-1 process retained the even and fined grain structure and the average grain diameter was reduced to $21 \mu\text{m}$ (Fig. 12 (d)).

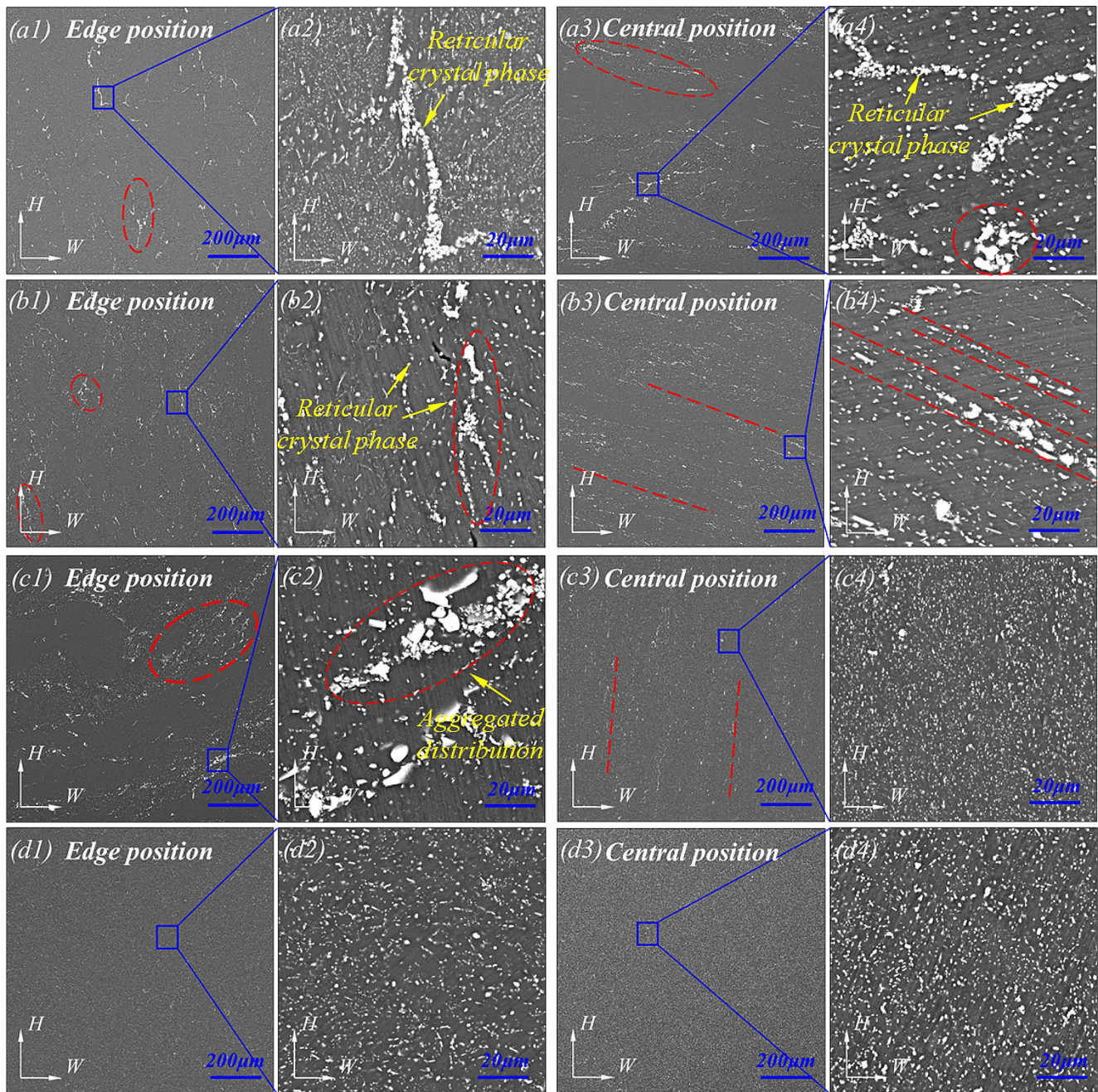


Fig. 7 SEM images of the edge and central position of 2195 Al-Li alloy in the transverse section after different MDF processes: (a1–a4) 400-4U3S-1; (b1–b4) 480-7U6S-2; (c1–c4) 480-7U6S-1; (d1–d4) 400-7U6S-1

3.2.3 Dislocation Evolution

To further analyze the grain refinement mechanism of the Al-Li alloy during MDF, the evolution of the dislocation configuration in different MDF processes was studied. Figure 13 shows the TEM images of the 2195 Al-Li alloy after different MDF processes. After adopting the MDF process of 400-4U3S-1 and 480-7U6S-2 process, the dislocation density in the samples was low, and only a few dislocation lines

were observed. However, there was a significant increase in the dislocation density of the 480-7U6S-1 samples. When the forging temperature of 400 °C and the forging method of 7U6S were adopted, the dislocation density in the matrix was considerably increased. Within the subgrain, a high density of dislocations was entangled and accumulated at the grain boundaries. Annealing in the MDF process eliminated a mass of dislocations, resulting in a significantly lower dislocation density in twice-heating forging than that

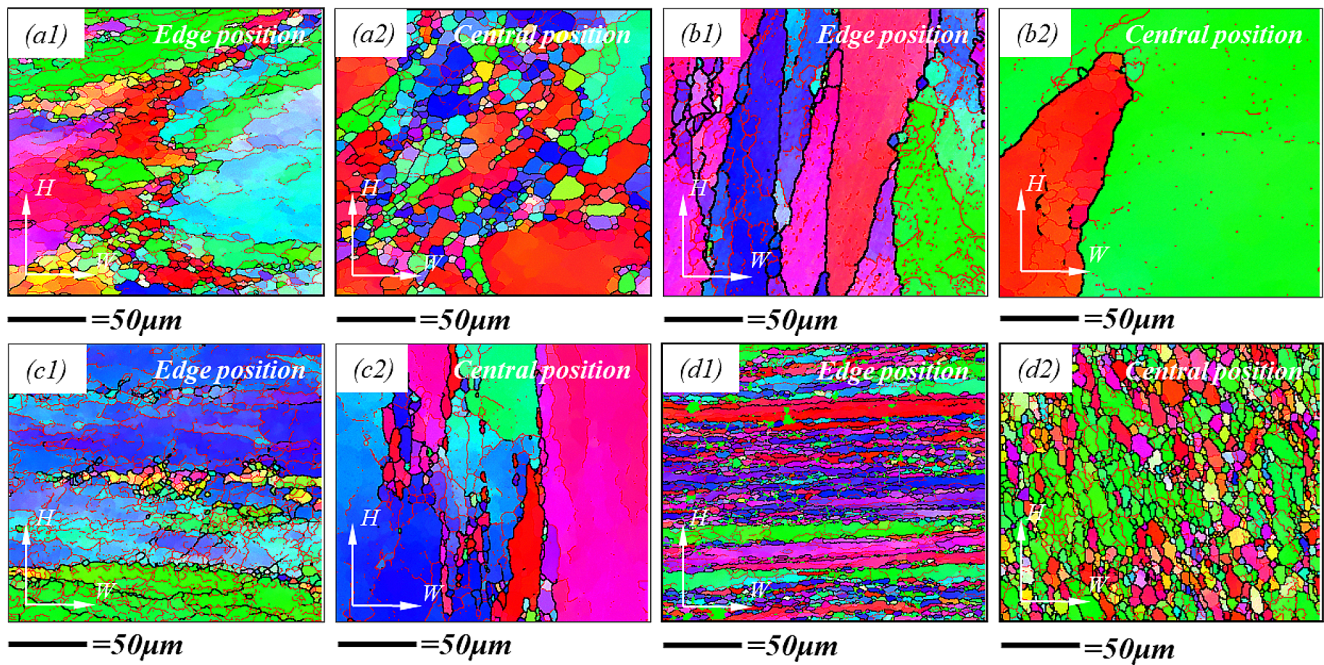


Fig. 8 EBSD images of the edge and center position of 2195 Al-Li alloy after different MDF processes: (a1, a2) 400-4U3S-1; (b1, b2) 480-7U6S-2; (c1, c2) 480-7U6S-1; (d1, d2) 400-7U6S-1

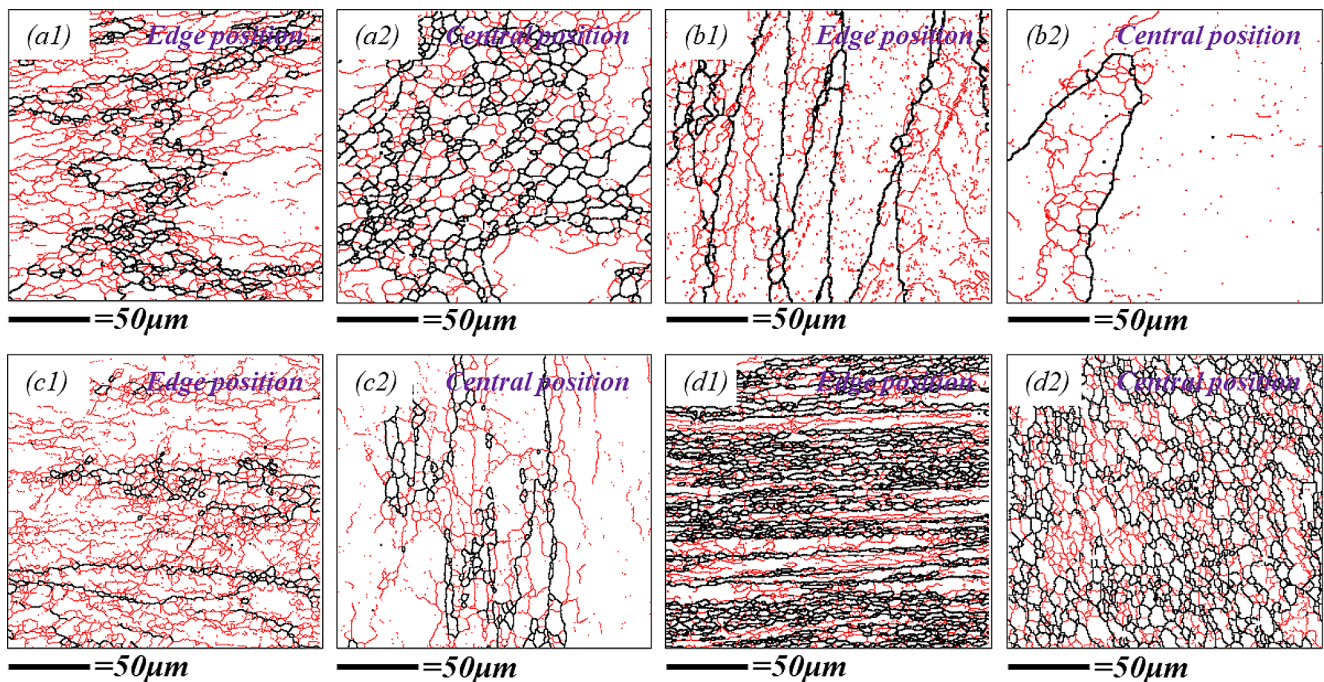


Fig. 9 Grain boundary images of the edge and center position of 2195 Al-Li alloy after different MDF processes: (a1, a2) 400-4U3S-1; (b1, b2) 480-7U6S-2; (c1, c2) 480-7U6S-1; (d1, d2) 400-7U6S-1

in the MDF process in the one heat forging process. As a result, reducing MDF temperature and increasing the number of upsetting and stretching significantly increased the dislocation density.

To quantitatively characterize the dislocation density, the samples of four MDF samples were analysed using the X-ray diffraction ($20^\circ < 2\theta < 90^\circ$), as shown in Fig. 14. The Williamson–Hall method was used to calculate the

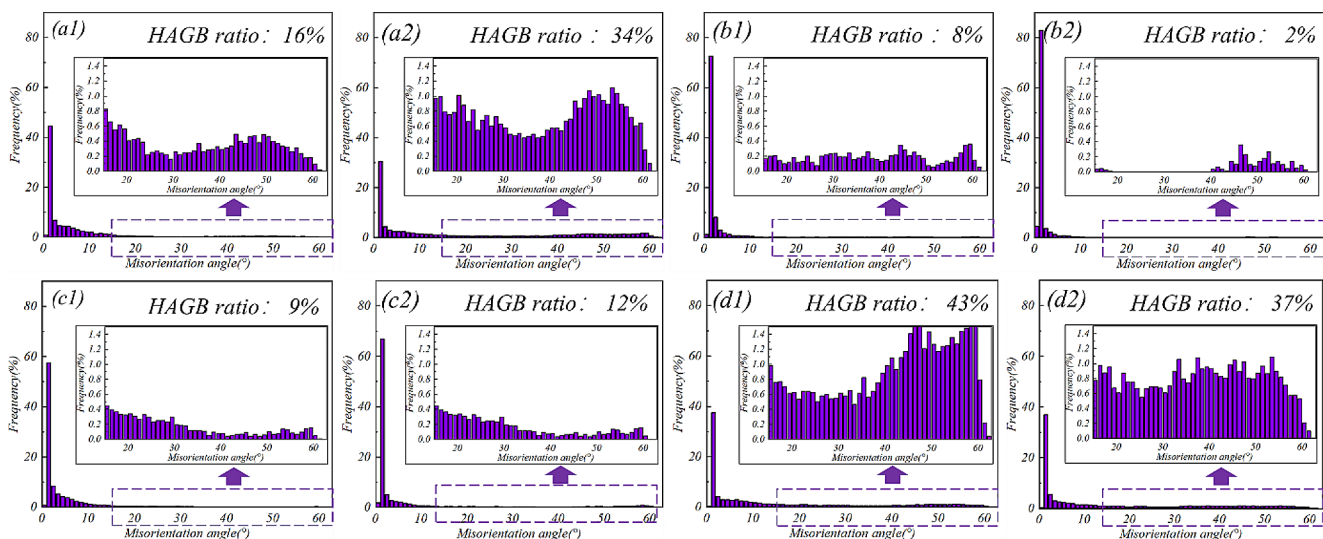


Fig. 10 Grain boundary distributions of the edge and center position of 2195 Al-Li alloy after different MDF processes: **(a1, a2)** 400-4U3S-1; **(b1, b2)** 480-7U6S-2; **(c1, c2)** 480-7U6S-1; **(d1, d2)** 400-7U6S-1

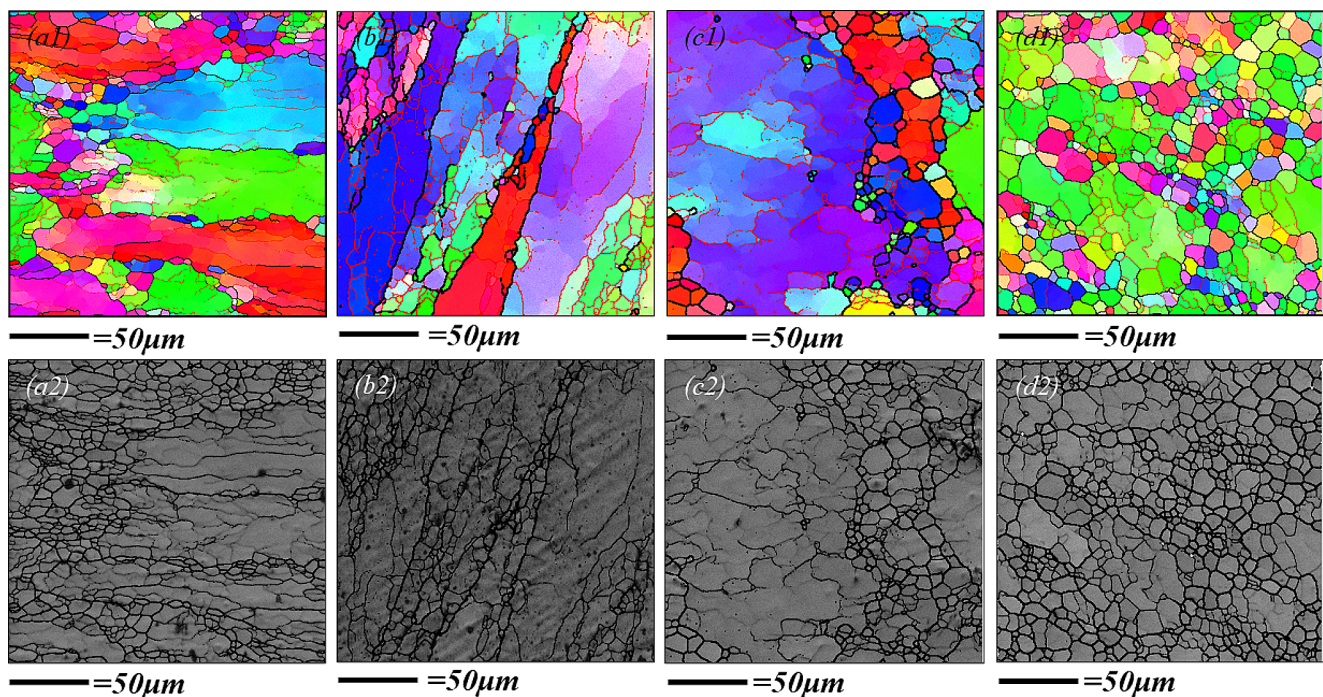


Fig. 11 EBSD images of the center position of 2195 Al-Li alloy after different MDF processes and annealing: **(a1, a2)** 400-4U3S-1; **(b1, b2)** 480-7U6S-2; **(c1, c2)** 480-7U6S-1; **(d1, d2)** 400-7U6S-1

dislocation density of the different MDF samples [28], as shown in Eq. 1:

$$\frac{\beta \cos \theta}{\lambda} = \frac{1}{D_v} + 2e \left(\frac{2 \sin \theta}{\lambda} \right) \quad (1)$$

where λ represents the wavelength of Cu $K\alpha$ radiation; θ is the diffraction angle; e and D_v represent the microstrain

and subgrain size, respectively. Therefore, e and D_v can be calculated by fitting the $(2 \sin \theta / \lambda)$ and $(\beta \cos \theta / \lambda)$. Then, the dislocation density (ρ) can be described as Eq. 2:

$$\rho = \frac{2\sqrt{3}e}{D_v b} \quad (2)$$

where b is the Burgers vector for Al alloy (0.285 nm). Using Eqs. 1 and 2, the dislocation density (ρ) of the 400-4U3S-1,

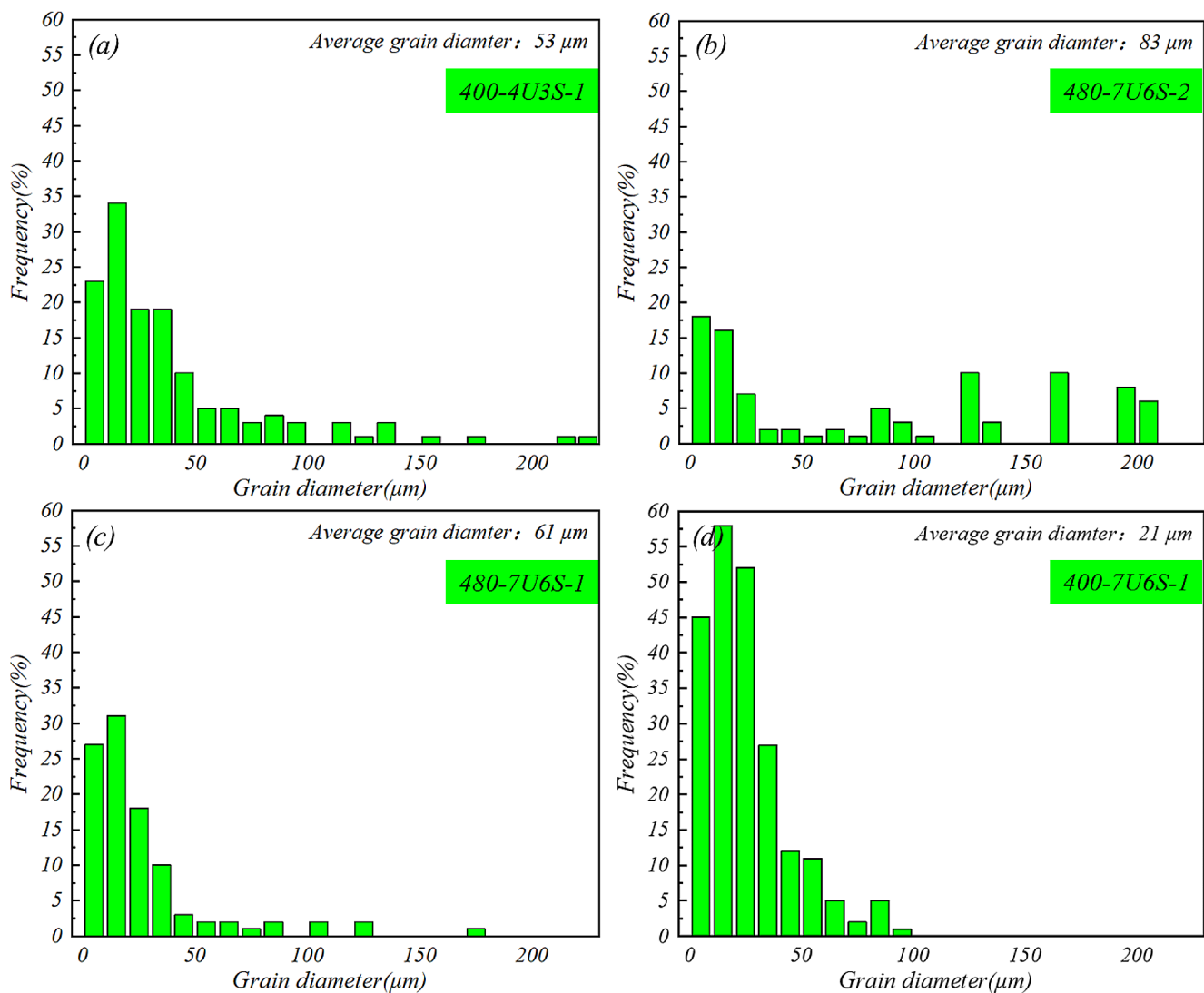


Fig. 12 Grain diameter distributions at the center position of 2195 Al-Li alloy after different MDF processes and annealing: (a) 400-4U3S-1; (b) 480-7U6S-2; (c) 480-7U6S-1; (d) 400-7U6S-1

480-7U6S-2, 480-7U6S-1, 400-7U6S-1 samples was calculated to be 4.3×10^{11} , 7.6×10^{11} , 1.2×10^{12} and 3.4×10^{13} m^{-2} , respectively. This was consistent with the evolution tendency of the dislocations observed using TEM.

3.3 Microstructures after T8 Heat Treatment

3.3.1 Evolution of Crystal Phases

SEM images of the 2195 Al-Li alloy forgings after solution treatment were obtained to analyse the evolution of the residual crystal phases during the final heat treatment. The results are shown in Fig. 15. After solution treatment at 500 °C for 4 h, a mass of fine secondary phase particles were dissolved into the matrix, while the coarse crystal phase particles were still difficult to dissolve completely. The samples

prepared using the MDF process of 400-7U6S-1 showed a significant decrease in the number of crystal phases, smaller size, and uniform distribution after solution treatment at both the edge and center. Nevertheless, the microstructure uniformity of the samples obtained using the other three MDF processes was poor after solution treatment. The crystal phases at the edges were still distributed along the grain boundaries. At the central position, the coarse crystal-phase particles aggregated along the direction of the flow. To quantitatively analyse the influence of the MDF process on the number of residual crystal phases, Image Pro-Plus software was used to calculate the area fraction of the coarse phase particles of the alloy. The statistical results are shown in Fig. 16. The 400-7U6S-1 samples had the lowest content of crystal-phase particles after solution treatment, and the area fraction of the particles at the edge and center was

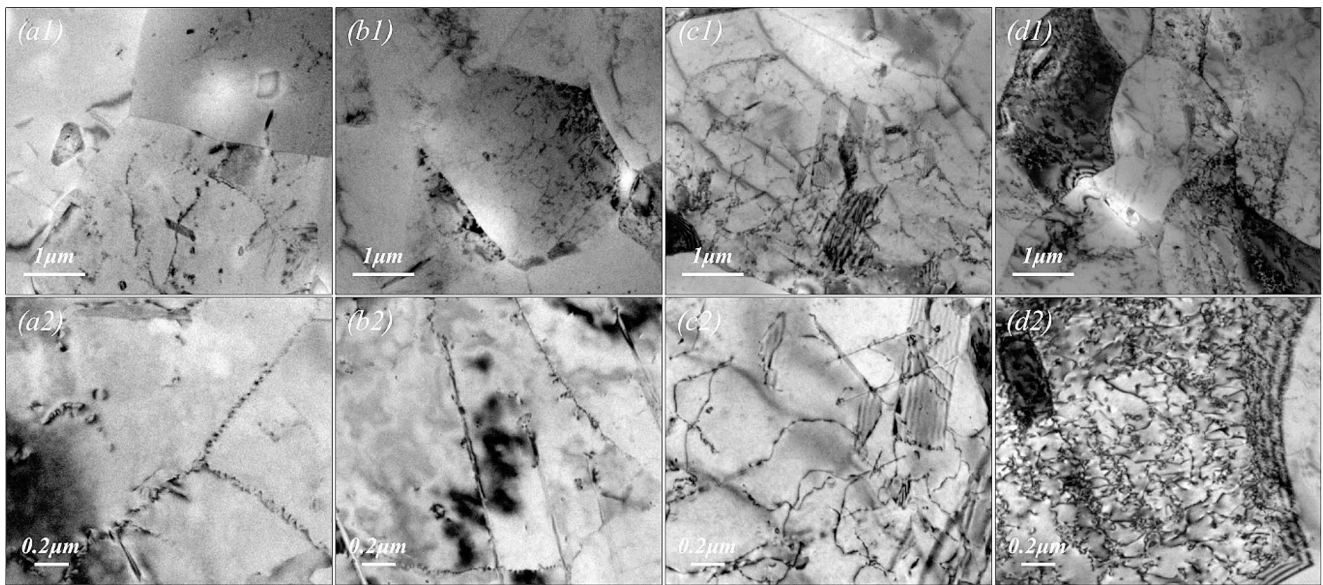
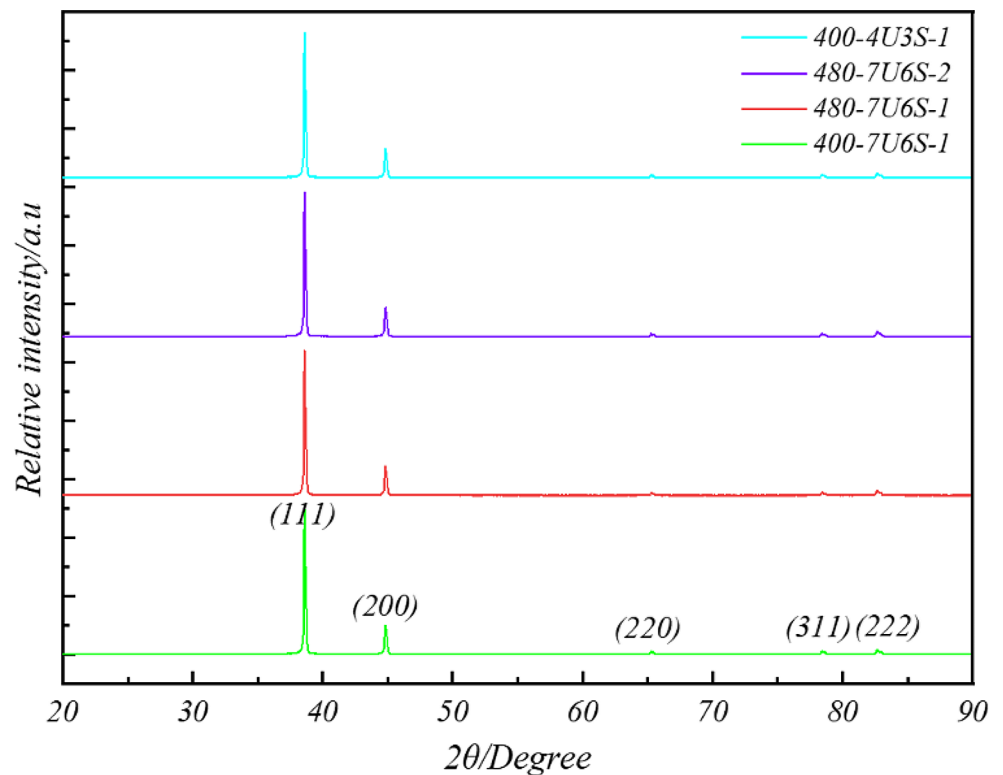


Fig. 13 TEM images of 2195 Al-Li alloy after different MDF processes: (a1, a2) 400-4U3S-1; (b1, b2) 480-7U6S-2; (c1, c2) 480-7U6S-1; (d1, d2) 400-7U6S-1

Fig. 14 XRD patterns of the 2195 Al-Li alloy after MDF



0.75% and 0.61%, respectively. However, the area fraction of the crystal-phase particles in the samples adopting the other three MDF processes was higher and the difference between the edge and central positions was larger.

3.3.2 Evolution of Grain Structure

Figure 17 shows the metallographic images of the 2195 Al-Li alloy forgings at different positions after T8 heat treatment. After the heat treatment, the grains of the sample in the transverse section were nearly equiaxial, and the grains in the central position of the longitudinal section were

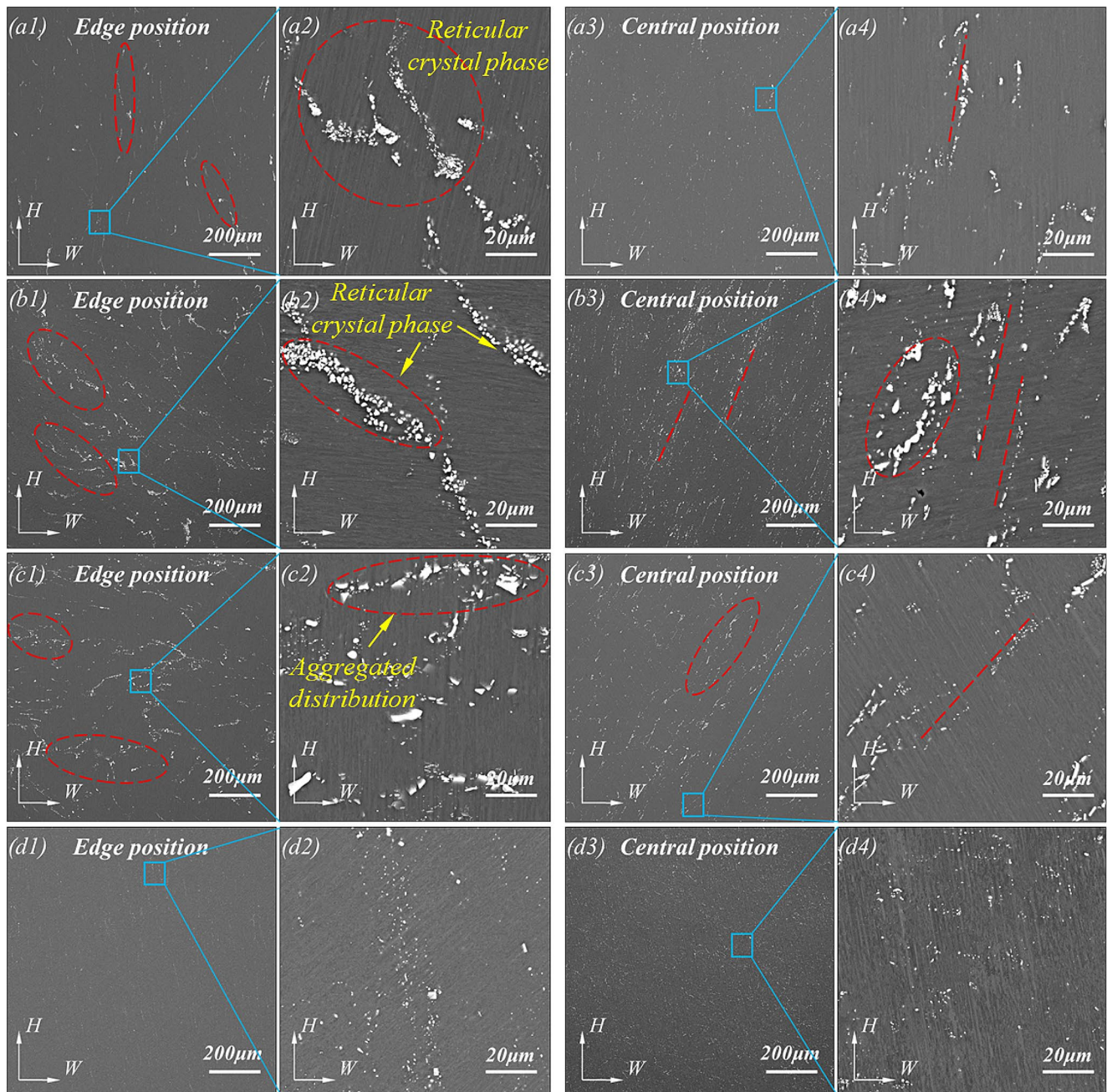


Fig. 15 SEM images of the edge and central position of 2195 Al-Li alloy forgings in the transverse section after solution treatment: **(a1–a4)** 400-4U3S-1; **(b1–b4)** 480-7U6S-2; **(c1–c4)** 480-7U6S-1; **(d1–d4)** 400-7U6S-1

elongated along the compression direction. The grains of the 400-4U3S-1 samples were coarse at different positions after heat treatment. In the transverse section, the grain size at the edge and center was 223 μm and 156 μm , respectively. In the longitudinal section, the grain size was slightly reduced and fine grains were observed at local locations. The grain sizes at the edge and center were 126 μm and 131 μm , respectively, which were close to the grain size of the ingot. When the number of upsetting and stretching was increased (MDF method was 7U6S), the grain was significantly refined after

heat treatment, and the diameter of most grains was reduced to 10–20 μm . However, abnormally coarse grains could still be observed in local regions. The size of abnormally coarse grain of the sample of 480-7U6S-2 process was nearly 120–150 μm , which was consistent with the grain size of the ingot. The coarse-grain size in the center of the 480-7U6S-1 sample was slightly reduced, ranging from 50 to 80 μm . However, the grains at the edges were still relatively coarse. In the MDF process of 400-7U6S-1, the grains in the edge and center of the samples were significantly refined to

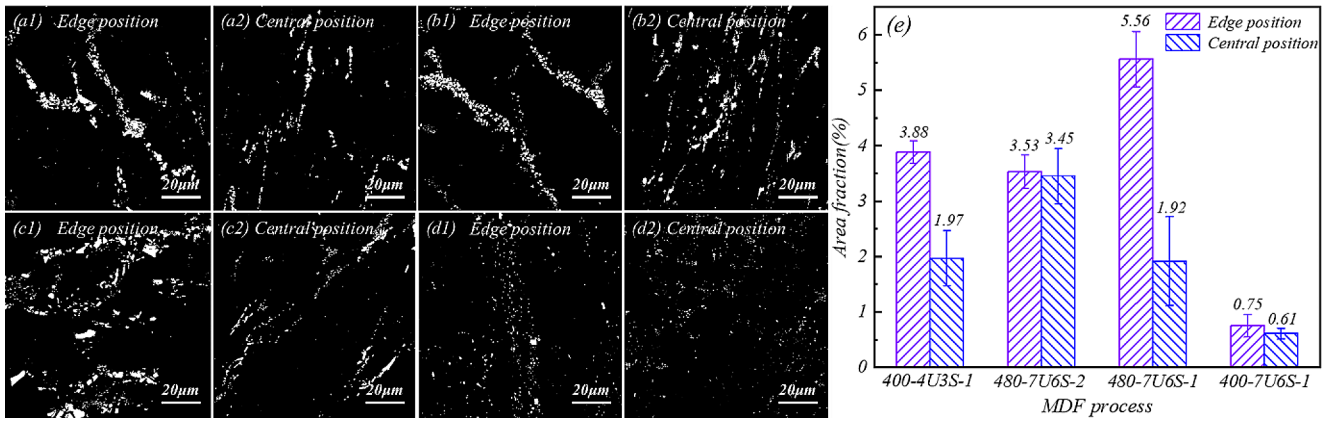


Fig. 16 Crystal phase particles of the edge and central position of the 2195 Al-Li alloy forgings in the transverse section after T8 heat treatment: (a1, a2) 400-4U3S-1; (b1, b2) 480-7U6S-2; (c1, c2) 480-7U6S-1; (d1, d2) 400-7U6S-1; (e) area fraction of crystal-phase particles

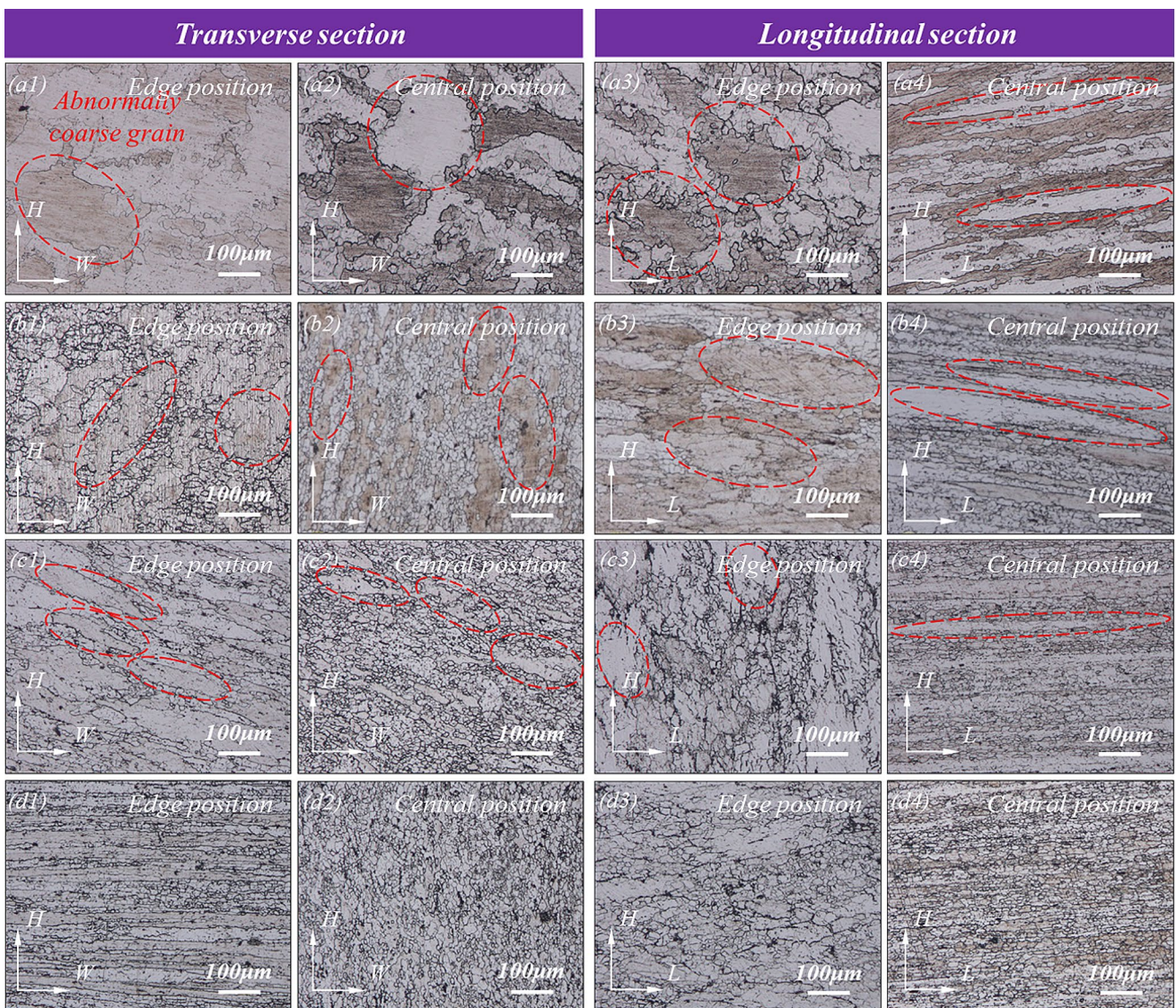


Fig. 17 Optical microscopy images of the edge and central position of 2195 Al-Li alloy forgings after T8 heat treatment: (a1–a4) 400-4U3S-1; (b1–b4) 480-7U6S-2; (c1–c4) 480-7U6S-1; (d1–d4) 400-7U6S-1

18 μm in different directions after T8 heat treatment, and no local abnormally coarse grains were observed. This indicates that the grain uniformity of the forgings was significantly improved.

3.3.3 Precipitated Phase Evolution

The TEM images and corresponding electron diffraction patterns of the T8-aged 2195 Al-Li alloy forgings observed along the $(110)_{\text{Al}}$ direction are shown in Fig. 18. Owing to the obvious T1 phase diffraction spots observed, the reinforced phases that precipitated during the aging of the 2195 Al-Li alloy were mainly needle-like T1 phases with a length distribution of 20–120 nm. According to the statistics obtained using the Image-ProPlus software, the area fraction of the T1 phases in the sample of 400-4U3S-1 was approximately 3.2%. The area fraction of the T1 phases in 480-7U6S-2 and 480-7U6S-1 samples increased to 4.3% when the MDF temperature and number of the upsetting and stretching were improved. Importantly, when the MDF process of 400-4U3S-1 was adopted, the precipitation force was significantly enhanced, and the area fraction of the T1 phase significantly increased to 6.7% (Fig. 18 (a4)). Furthermore, the weak δ' phase diffraction spots in the electron diffraction spot images indicated that the spherical phases observed in the sample using the MDF process of 400-4U3S-1 and 480-7U6S-2 were the δ' phase.

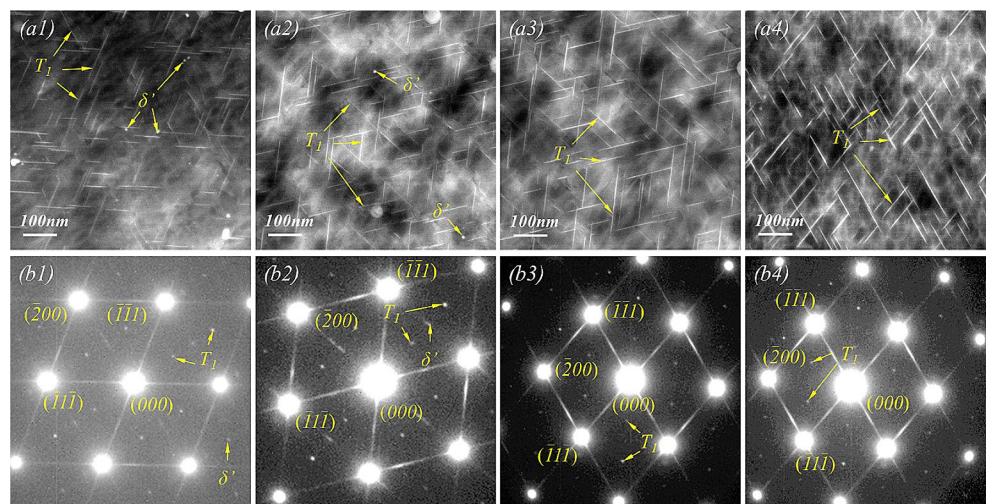
3.4 Three-Directional Mechanical Properties and Fracture Characteristics

The mechanical properties of the forgings after T8 heat treatment were tested in the width, height and length directions at different positions, as shown in Fig. 19. The mechanical properties of MDF forging using the 400-4U3S-1 process were the worst, with an average tensile strength (TS), yield

strength (YS) and elongation (EL) of 558 MPa, 513 MPa and 4.3%, respectively, and the elongation in the height direction was only 2.4%. Additionally, the three-directional mechanical properties exhibited significant anisotropy, and the maximum differences in TS, YS and EL were 15 MPa, 26 MPa and 2.1%, respectively. Adopting the 480-7U6S-2 and 480-7U6S-1 processes significantly improved the three-directional strength and elongation. Nevertheless, the elongation in the height direction was low at only 3.5% and 3.2%, respectively. The strength and toughness of the forgings using the MDF process with 400-7U6S-1 were further improved. Compared to the MDF process of 400-4U3S-1, the TS in the width, height and length directions increased by 40 MPa, 32 MPa and 35 MPa, respectively. The YS in the three directions increased by 37 MPa, 39 MPa and 25 MPa, respectively, and the strength difference at the different positions was less than 10 MPa. Notably, the elongation in the height direction of the T8-aged forgings increased significantly from 2.4 to 6.3%, and the elongation in the width and length directions increased to 8% and 9.8%, respectively. Therefore, the MDF process of 400-7U6S-1 can achieve a higher toughness and performance uniformity (Table 2), and this process is expected to be used in the cogging of 2195 Al-Li alloy rings for launch vehicle fuel tanks.

To further analyse the factors affecting the fracture behaviour of the Al-Li alloy, the fracture surfaces of the tensile specimens were observed. Figures 20, 21 and 22 show SEM images of the fracture of the tensile specimens at different positions of the 2195 Al-Li alloy forgings. It can be observed that nearly all the fracture surfaces of the samples at the edge and center using the MDF processes of 400-4U3S-1 and 480-7U6S-2 presented rock sugar-like fracture characteristics, which were obvious intergranular fractures, and a certain degree of second-phase particles could be observed at the grain boundaries (Fig. 22 (a1–a2, b1–b2)). The fracture at the edge of the sample using the

Fig. 18 TEM images and corresponding electron diffraction patterns of the 2195 Al-Li alloy forgings after different MDF processes and T8 heat treatment: (a1, b1) 400-4U3S-1; (a2, b2) 480-7U6S-2; (a3, b3) 480-7U6S-1; (a4, b4) 400-7U6S-1



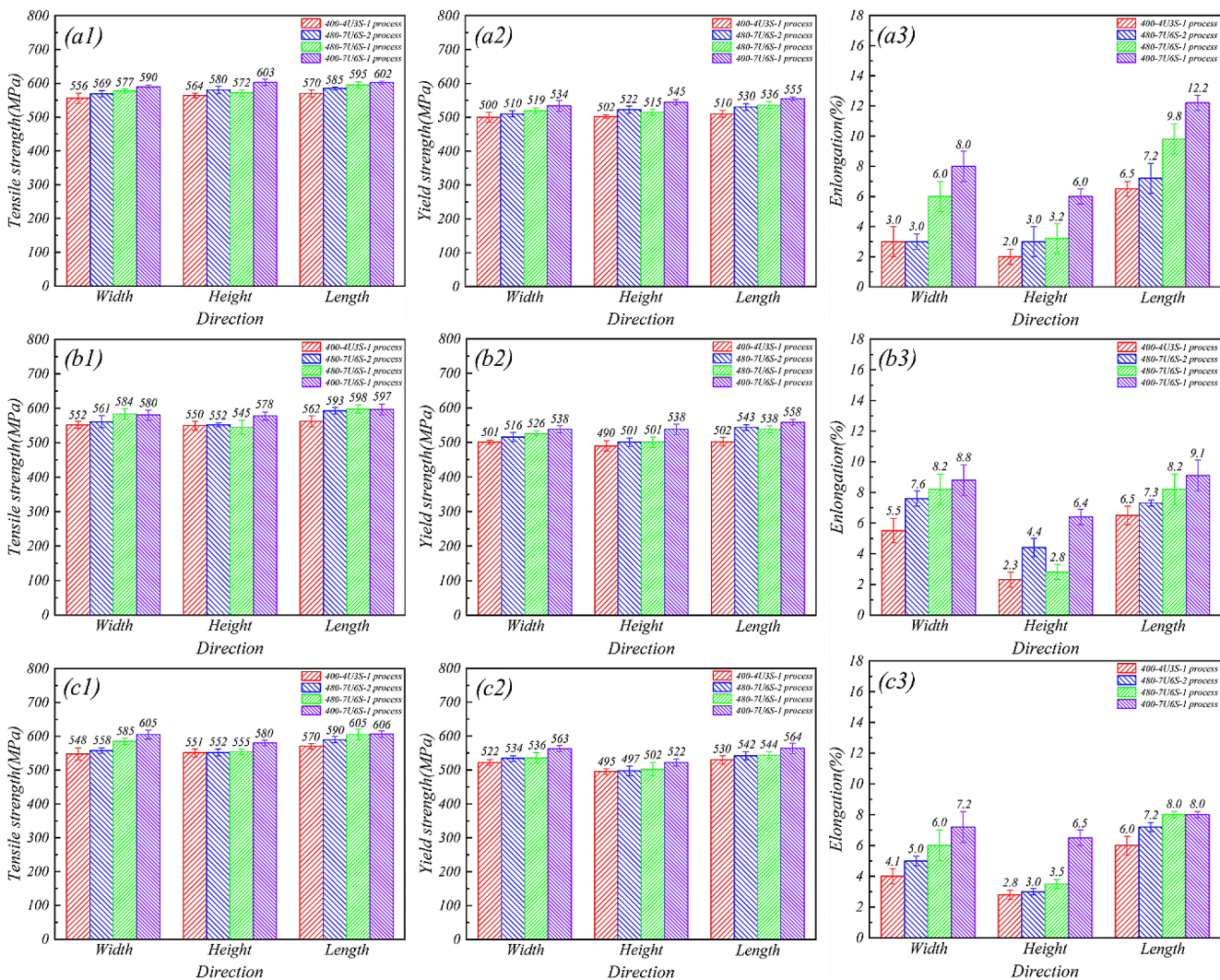


Fig. 19 Three-directional mechanical properties of T8-aged 2195 Al-Li alloy forgings at different positions: (a1–a3) edge position, (b1–b3) quarter position, and (c1–c3) central position

Table 2 Average value of three-directional mechanical properties of 2195 Al-Li alloy forgings

MDF process	Properties	Width	Height	Length
400-4U3S-1	Tensile strength	552	555	567
	Yield strength	508	496	534
	Elongation	4.2	2.4	6.3
480-7U6S-2	Tensile strength	563	561	589
	Yield strength	520	517	507
	Elongation	5.2	3.5	7.2
480-7U6S-1	Tensile strength	582	557	599
	Yield strength	527	506	539
	Elongation	6.7	3.2	8.7
400-7U6S-1	Tensile strength	592	587	602
	Yield strength	545	535	559
	Elongation	8	6.3	9.8

480-7U6S-1 process was still characterized by a rock-sugar-like intergranular fracture. At the central position, a small number of dimples and a large number of second-phase particles can be observed (Fig. 22 (c1, c2)). This indicates the occurrence of transgranular fractures in local regions. However, the edge and center of the sample prepared using the 400-7U6S-1 process presented mainly transgranular fractures, and the intergranular fracture area was significantly reduced. Additionally, the diameters of the second-phase particles at different fracture positions decreased significantly from 6.3 μm to 1.1 μm (Fig. 22 (d1, d2)).

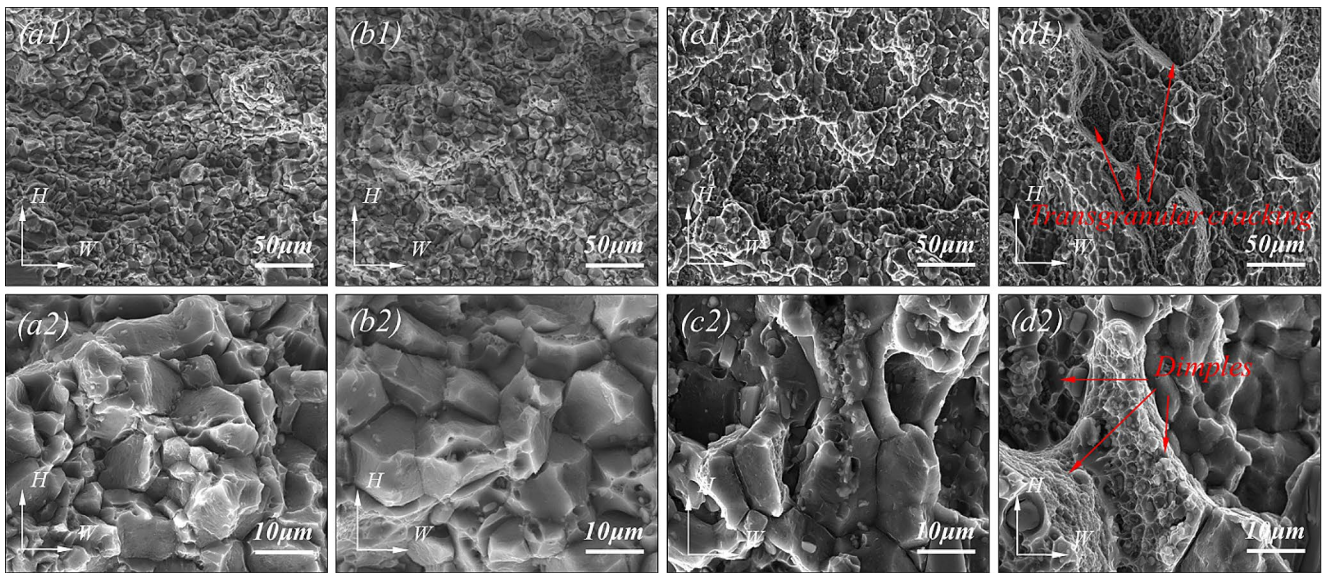


Fig. 20 SEM images of tensile fracture surfaces at the center of T8-aged 2195 Al-Li alloy forgings under the different MDF processes: (a1, a2) 400-4U3S-1; (b1, b2) 480-7U6S-2; (c1, c2) 480-7U6S-1; (d1, d2) 400-7U6S-1

Fig. 21 SEM images of tensile fracture surfaces at the edge of T8-aged 2195 Al-Li alloy forgings under the different MDF processes: (a1, a2) 400-4U3S-1; (b1, b2) 480-7U6S-2; (c1, c2) 480-7U6S-1; (d1, d2) 400-7U6S-1

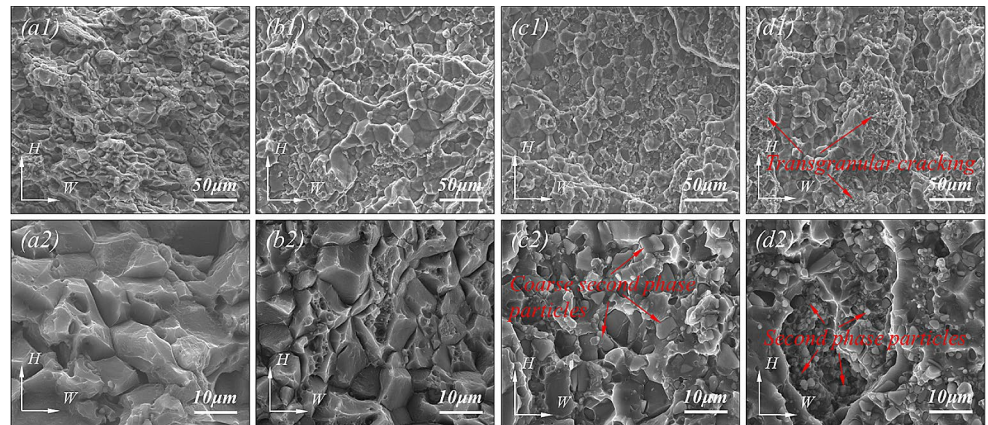
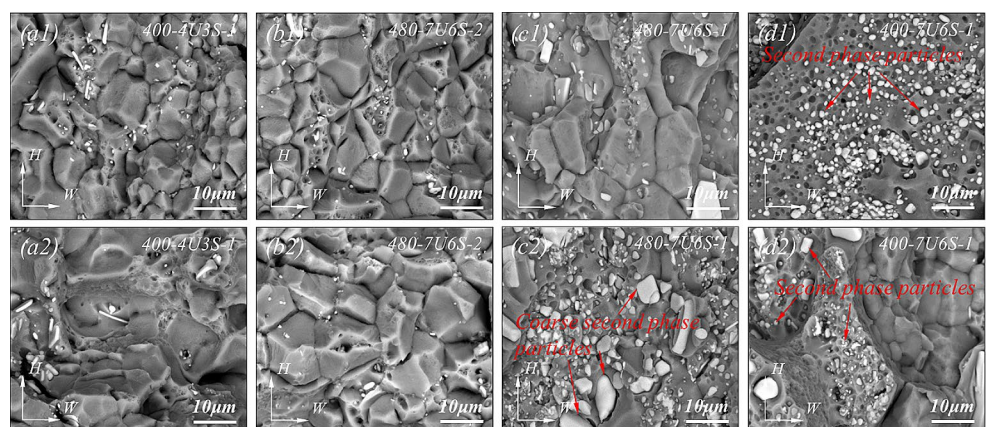


Fig. 22 Second-phase particle distribution in the tensile fracture surfaces of T8-aged 2195 Al-Li alloy forgings at the: (a1–d1) edge position; (a2–d2) central position



4 Discussion

4.1 Microstructural Evolution

4.1.1 Crystal Phases Dispersing by Strong Deformation during MDF at 400 °C

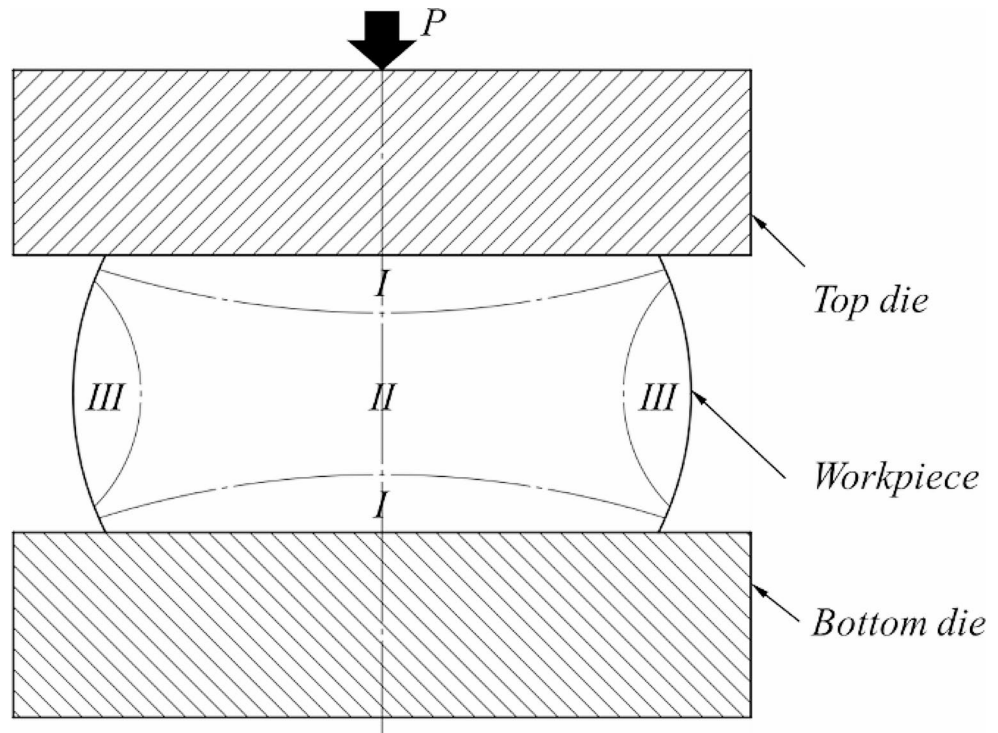
During the upsetting process, the deformation of the billet at each position was not uniform (Fig. 23), and the deformation zones included stagnant, easily deformed, and freely deformed zones [29].

It has been confirmed that the uneven reticular crystal phases formed by segregation during the casting process were inherited by the final forging after heat treatment, which significantly reduced the mechanical properties and uniformity of the forging [30]. Figure 7 shows that compared to the MDF process of 4U3S, the 7U6S process was more beneficial for improving the reticular structure of the crystal-phase particles. Because the 7U6S process increased the number of upsetting and drawing, a greater degree of plastic strain was obtained, and the fracture stress of the crystal phases at the grain boundaries was increased. However, increasing the heating number was not conducive to confirming the distribution of the crystal phases. The recovery that occurred during the intermediate annealing process eliminated many dislocations generated by the thermal deformation process, resulting in a decrease in the stress level around the crystal phases, which was not sufficient to break the coarse particles. The strong deformation resistance produced during the forging at 400 °C not only increased the crushing stress

of the second-phase particles, but also increased the deformation of the edge of the alloy and improved deformation inhomogeneity. This completely eliminated the reticular structure of the crystal phases between the edge and center of the alloy, resulting in a uniform and dispersed microstructure (Fig. 7(d1–d4)). Therefore, the MDF process of 400-7U6S-1 proposed in this study had a significant effect on the uniformity and dispersion control of coarse reticular crystal phases, which prevented their inheritance in the final forging.

Studies have shown that dislocations can provide channels for the diffusion of second-phase particles at high temperatures [31]. The strong lattice distortion and higher density of dislocations produced by the MDF process of 400-7U6S-1 provided a diffusion channel for the crystal-phase particles smashed during MDF, which facilitated the dissolution of a large number of crystal-phase particles during the subsequent high-temperature annealing process and significantly reduced the crystal phases at the sample edges and center (Fig. 15(d1–d4)). Simultaneously, with the dissolution of the residual crystal phases, the saturation of the matrix increased, which significantly enhanced the precipitation force of T1 phases in the subsequent aging process. Thus, dispersed T1 phases with higher density were obtained using the MDF process of 400-7U6S-1 (Fig. 18(a4)).

Fig. 23 Diagram of deformation zones of the upsetting process: I stagnant zone, II easy-deformation zone, III free-deformation zone



4.1.2 Dynamic Recrystallization with Uniform Nucleation during MDF Refined the Grains

Under the condition that the alloy does not crack during the forging process, the deformation resistance of Al-matrix was significantly enhanced by reducing the MDF temperature to 400 °C and increasing the number of upsetting and stretching. This accelerated the rate of dislocation accumulation and resulted in an extremely high dislocation density in the matrix (Fig. 13). These dislocations enhanced the stored energy of the alloy and form more uniform high-energy regions, which increased the degree of dynamic recrystallization during the MDF process. Furthermore, studies have confirmed that second-phase particles can stimulate nucleation (PSN) [32]. The strong deformation resistance of the MDF process of 400-7U6S-1 caused the second-phase particles to disperse, which provided favourable conditions for uniform nucleation and thus resulted in fine and uniform dynamic recrystallization grains (Fig. 8 (d1, d2)). Because the Al₃Zr particles in 2195 Al-Li alloy can inhibit recrystallization [33] and the high-temperature recovery and dynamic recrystallization during thermal deformation consume a large number of dislocations, they are insufficient to provide a sufficient driving force for static recrystallization during the solution process. Consequently, recrystallization during the final heat treatment process was inhibited, and fine and uniform dynamic recrystallization grains were retained (Fig. 8 (d1-d4)).

However, improving the MDF temperature to 480 °C, reducing the number of upsetting and stretching and increasing the heating number of forging reduced the dislocation density in the matrix, which reduced the nucleation rate and enhanced the non-uniformity of the deformation of the edge and center of the forging. Meanwhile, the aggregation of the second-phase particles and the low nucleation rate caused uneven nucleation, which resulted in grain boundaries at local locations not being restricted by the surrounding grains during the grain growth process of dynamic recrystallization. Eventually, the grain boundary migration rate accelerated and abnormally coarse grains were formed (Fig. 24).

4.2 Analysis of Three-Dimensional Mechanical Properties

4.2.1 Strength

The 2195 Al-Li alloy is a deformed alloy that can be strengthened by heat treatment, and the main strengthened phase that precipitated during the aging process is the T1 phases. The strength improvement caused by the T1 phases can be expressed as follows [34]:

$$\sigma = 0.13MG \frac{b}{2\sqrt{lt}} \left[\sqrt{f} + 0.75f \left(\frac{l}{t} \right)^{\frac{1}{2}} + 0.14\sqrt{f^3} \left(\frac{l}{t} \right) \right] \ln \left(\frac{0.158L}{r_o} \right) \quad (3)$$

where σ is the yield strength associated with T1 phase; G is the shear modulus (~27 GPa); M is the Taylor factor (usually taken as 3.1); r_o is the inner radius of dislocation around the T1 phase; b is the Burgers vector of Al alloy (0.285 nm); and l , t , and f are the length, thickness, and volume fraction of the T1 phase, respectively. As mentioned previously, the MDF process of 400-7U6S-1 combined with high temperature annealing caused numerous of second-phase particles to break and dissolve in the matrix, which increased the saturation of the solid solution and the aging precipitation force of the T1 phases. The volume fractions (f) of the T1 phases for the four specimens were measured using image-proplus software and were 3.53%, 4.16%, 4.23% and 5.38%, respectively. The thickness (t) of the T1 phases in the four samples was almost unchanged at ~12 nm, while the average length (l) of 400-7U6S-1 samples was reduced from 96 nm to 83 nm. According to Eq. 3, the increment of yield strength compared to 400-4U3S-1 samples can be calculated as 21 MPa, 23 MPa and 55 MPa respectively, which was basically consistent with the experimental results. Therefore, the precipitation of the higher density T1 phases was key factor for the significant strength improvement of Al-Li alloy.

In addition, the MDF process of 400-7U6S-1 refined the grain structure, eliminated the abnormal coarse grains that were easily formed in local positions owing to uneven deformation, and obtained fine and uniform dynamic recrystallization grains. Therefore, an increase in the total area of the grain boundaries leads to an increase in the resistance to dislocation movement, which is another important factor for the strength improvement of the alloy.

4.2.2 Ductility

As can be seen from Figs. 20–22, the fractures of the forgings adopting the MDF process of 400-4U3S-1 and 480-7U6S-2 show obvious fracture characteristics of the crystal sugar shape, which is typical intergranular fracture behaviour and the elongation in the direction of height and width was only 3–5%. A large number of dimples appeared on the fracture surface of the samples adopting the MDF process of 400-7U6S-1, which indicated that the fracture behaviour of the alloy gradually changed to transgranular fracture and the elongation in the direction of height and width increased by 6–8%. Because the 400-4U3S-1 and 480-7U6S-2 processes was difficult to effectively eliminate the reticular structure

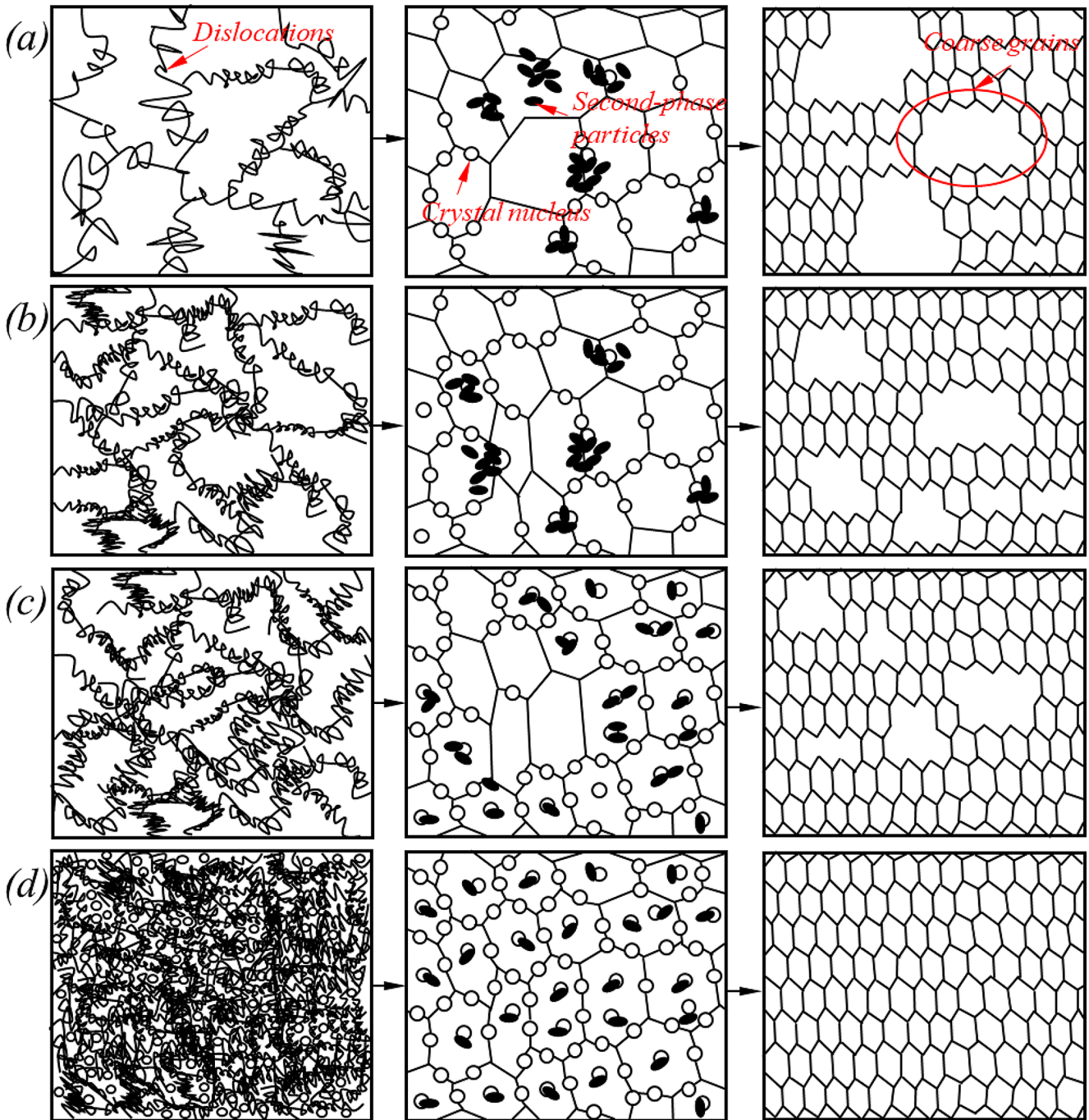


Fig. 24 Schematic of grain structure evolution of 2195 Al-Li alloy forgings after different MDF processes and heat treatment: (a) 400-4U3S-1; (b) 480-7U6S-2; (c) 480-7U6S-1; (d) 400-7U6S-1

of the crystal phases during MDF, a large number of coarse second-phase particles were still distributed along the grain boundaries after the final heat treatment. When the alloy was loaded, a high stress concentration was easily produced around the gathered second-phase particles, forming cracks at the grain boundaries. The MDF process of 400-7U6S-1 dispersed the second-phase particles to reduce the stress concentration and avoid the formation of microcracks. By

contrast, the fine and uniform grain structure increased the area of the grain boundaries, which reduced the crack propagation rate and improved the plasticity of the alloy. Conversely, the inhibitory effect of abnormally coarse grains formed by non-uniform nucleation on crack growth was reduced, which was the key to reducing the ductility of the alloy. Moreover, studies have shown that the δ' phase (Al_3Li) can cause coplanar slip of the dislocation during

the deformation, resulting in a decrease in plasticity [35]. According to Fig. 17, the MDF process of 400-7U6S-1 combined with high-temperature annealing enhanced the precipitation force of the T1 phase (Al_2CuLi) and inhibited the precipitation of δ' phase, and thus the ductility of the alloy was improved.

In summary, the uniform fine grains and dispersed second phases produced by the MDF process of 400-7U6S-1 reduced the stress concentration and crack propagation rate, and thus significantly improved the plasticity of the Al-Li alloy.

5 Conclusions

In this study, the effect of the MDF process on the microstructure and three-directional mechanical properties at the edge and center of 2195 Al-Li alloy was studied systematically and an improved MDF process was proposed. The main conclusions are as follows:

(1) The strong deformation resistance caused by reducing the MDF temperature to 400 °C and increasing the number of upsetting and stretching (7U6S) made the coarse crystal phases at the edge and center of Al-Li alloy to be sufficiently broken, which completely eliminated the reticular structure of the crystal phases. The dispersive distribution of the crystal phases reduced the stress concentration around the second-phase particles at the grain boundaries, effectively preventing intergranular fracture and significantly improving the plasticity of the alloy.

(2) The abundant dislocations formed by the MDF process of 400-7U6S-1 promoted the dissolution of more dispersed crystal-phase particles into the matrix during the solution process, and the area fraction of the crystal phase at the edge and center of the alloy was significantly reduced from 3.88 to 0.75% and 1.97–0.61%, respectively. The dissolution of a mass of crystal phases enhanced the precipitation force of the T1 phases during aging and increased the density of the precipitated phase, significantly improving the strengthening ability of the 2195 Al-Li alloy.

(3) Compared with the MDF processes of 400-4U3S-1, 480-7U6S-2 and 480-7U6S-1, the 400-7U6S-1 process resulted in a higher density of dislocations and more dispersed second-phase particles, which provided a favourable position for the uniform nucleation of recrystallized grains and significantly improved the dynamic recrystallization nucleation rate during the MDF process. The average grain diameter of the alloy was refined from 159 μm to 17 μm . This process eliminated the abnormally coarse grains formed by uneven nucleation, which improved the homogeneity of the structure and obtained a uniform ultrafine grain structure.

(4) Compared to the conventional MDF process of 400-4U3S-1, the uniform ultra-fine grain structure and dispersed precipitated phases obtained by the 400-7U6S-1 process significantly improved the mechanical properties of the 2195 Al-Li alloy forgings. The tensile strengths of width, height and length increased from 552 MPa, 555 MPa and 567 MPa to 592 MPa, 587 MPa and 602 MPa, respectively, which were increases of 7.2%, 5.8% and 6.2%, respectively, and the yield strengths in the three directions improved from 508 MPa, 495 MPa and 534 MPa to 545 MPa, 535 MPa and 559 MPa, respectively, which were 7.2%, 8.0% and 4.7% higher, respectively. Importantly, the elongation in the three directions markedly increased from 4.2%, 2.4% and 6.3–8.0%, 6.3% and 9.8%, with increases of 90.5%, 162.5% and 55.6%, respectively. Furthermore, the maximum difference in elongation at different positions in the width direction was reduced from 83.3 to 11.1%, which significantly improved the ductility uniformity of the Al-Li alloy.

Acknowledgements This work was funded by the Joint Funds of the National Natural Science Foundation of China (Grant No. U21B6004), the Major Projects of Scientific and Technology Innovation of Hunan Province (Grant No. 2021GK1040) and the Research Project of State Key Laboratory of Precision Manufacturing for Extreme Service Performance in China (Grant No. ZZYJKT2023-03). We would like to thank Editage (www.editage.cn) for English language editing.

Declarations

Competing Interests The authors declare that they have no known competing financial interests or personal relationships that could have appeared to influence the work reported in this paper.

References

1. X. Zhang, Y. Chen, J. Hu, Recent advances in the development of aerospace materials. *Prog. Aero. Sci.* **97**, 22–34 (2018)
2. P. Lv, R. Wang, C. Peng, Z. Cai, Microstructural evolution and mechanical properties of 2195 Al-Li alloy processed by rapid solidification and thermo-mechanical processing. *J. Alloys Compd.* **948**, 169794 (2023)
3. E.A. Hajjioui, K. Bouchaala, M. Faqir, E. Essadiqi, A review of manufacturing processes, mechanical properties and precipitations for aluminum lithium alloys used in aeronautic applications. *Heliyon* **9**, e12565 (2023)
4. Q. Pu, Z. Jia, Y. Kong, Q. Yang, Z. Zhang, X. Fan, H. Zhang, L. Lin, Q. Liu, Microstructure and mechanical properties of 2195 alloys prepared by traditional casting and spray forming. *Mater. Sci. Eng. A* **784**, 139337 (2020)
5. M. Qi, C. Chen, J. Wei, X. Mei, C. Sun, G. Su, C. Zhang, M. Yan, F. Yang, Z. Guo, Superior mechanical properties and microstructural evolution of powder metallurgy 2195 Al-Li alloy subjected to hot extrusion. *J. Alloys Compd.* **962**, 171184 (2023)
6. Y. Wang, G. Wu, L. Zhang, Y. Guo, C. Wang, L. Li, X. Xiong, Microstructure evolution and mechanical properties of a cast and heat-treated Al-Li-Cu-Mg alloy: Effect of cooling rate during casting. *Mater. Sci. Eng. A* **880**, 145366 (2023)

7. L. Zhang, X. Li, R. Li, R. Jiang, L. Zhang, Effects of high-intensity ultrasound on the microstructures and mechanical properties of ultra-large 2219 Al alloy ingot. *Mater. Sci. Eng. A* **763**, 138154 (2019)
8. Y. Zhang, R. Li, P. Chen, X. Li, Z. Liu, Microstructural evolution of Al₂Cu phase and mechanical properties of the large-scale Al alloy components under different consecutive manufacturing processes. *J. Alloys Compd.* **808**, 151634 (2019)
9. Z. Niu, G. Liu, T. Li, S. Ji, Effect of high pressure die casting on the castability, defects and mechanical properties of aluminum alloys in extra-large thin-wall castings. *J. Mater. Res. Technol.* **303**, 117525 (2022)
10. H. He, Y. Yi, S. Huang, Y. Zhang, Effects of deformation temperature on second-phase particles and mechanical properties of 2219 Al-Cu alloy. *Mater. Sci. Eng. A* **712**, 414–423 (2018)
11. X. Mao, Y. Yi, H. He, S. Huang, W. Guo, H. Lin, J. Que, Effects of warm saddle forging deformation on the reduction of second-phase particles. *Mater. Sci. Eng. A* **804**, 140737 (2021)
12. X. Mao, Y. Yi, H. He, S. Huang, W. Guo, Second phase particles and mechanical properties of 2219 aluminum alloys processed by an improved ring manufacturing process. *Mater. Sci. Eng. A* **781**, 139226 (2020)
13. S. Karimi, N. Fakhar, M. Faraji, F. Fereshteh-Saniee, Simultaneous improvement of mechanical strength and corrosion resistance in aluminum alloy 5083 via severe plastic deformation. *Mater. Chem. Phys.* **313**, 128755 (2024)
14. F. Cao, R. Liu, S. Kong, N. Guo, P. Xu, G. Xu, Microstructural evolution, high temperature tensile deformation behavior, and deformation mechanism in an Mg–Zn–Y–Ca–Zr alloy processed by multidirectional forging and hot rolling. *J. Mater. Res. Technol.* **27**, 6729–6743 (2023)
15. A. Rezaei, R. Mahmudi, C. Cayron, R.E. Logé, Simple shear extrusion versus equal channel angular pressing: a comparative study on the microstructure and mechanical properties of an mg alloy. *J. Magnes. Alloys* **11**, 1769–1790 (2023)
16. T. Masuda, Y. Tang, I.F. Mohamed, Z. Horita, Ultrafine-grained AZ61 alloy produced by high-pressure torsion: Advent of superplasticity and effect of anisotropy. *Mater. Sci. Eng. A* **879**, 145240 (2023)
17. A. Farokhpey, M.H. Parsa, Analyzing the accumulative roll bonding deformation zone behavior by FEM, upper bound, and experimental methods. *J. Manuf. Process.* **81**, 328–345 (2022)
18. Z. Zhang, L. Yuan, M. Zheng, Q. Wei, D. Shan, B. Guo, Achievement of high strength and good ductility in the large-size AZ80 mg alloy using a designed multi-directional forging process and aging treatment. *J. Mater. Res. Technol.* **311**, 117828 (2023)
19. J. Zhao, H. Guo, T. Luo, C. Zhang, J. Luo, Microstructure evolution and grain refinement mechanism of fine-grained Mg–Gd–Y–Zn–Zr alloy during multi-directional forging. *J. Alloys Compd.* **928**, 167199 (2022)
20. J. Zhang, H. Xie, Z. Lu, Y. Ma, S. Tao, K. Zhao, Microstructure evolution and mechanical properties of AZ80 magnesium alloy during high-pass multi-directional forging. *Result Phys.* **10**, 967–972 (2018)
21. J. Wang, C. Liu, S. Jiang, G. Zeng, Microstructure, texture evolution and mechanical properties of a large-scale multidirectionally forged Mg–Gd–Y–Zn–Zr–Ag alloy. *J. Mater. Res. Technol.* **24**, 3548–3563 (2023)
22. B. Wang, Y. Yi, H. He, S. Huang, Effects of deformation temperature on second-phase particles and mechanical properties of multidirectionally-forged 2A14 aluminum alloy. *J. Alloys Compd.* **871**, 159459 (2021)
23. A.V. Mikhaylovskaya, M.S. Kishchik, A.D. Kotov, N.Y. Tabachkova, Grain refinement during isothermal multidirectional forging due to β -phase heterogenization in Al–Mg-based alloys. *Mater. Letter.* **321**, 132412 (2022)
24. C. Cui, J. He, W. Wang, W. Chen, W. Zhang, Microstructure, texture and mechanical properties of extruded AZ31 mg alloy during small strain multi-directional forging with gradient cooling. *J. Alloys Compd.* **909**, 164795 (2022)
25. J. Sun, X. Wang, J. Li, D. Shu, S. Wang, P. Peng, Q. Mao, T. Liu, X. Lu, Y. Li, D. Zhu, G. Wang, W. Qin, Enhanced mechanical properties of ultrafine-lamella 304L stainless steel processed by multidirectional hot forging. *Vacuum* **187**, 110116 (2021)
26. P.C. Alves Flausino, E.C. Siqueira Corrêa, P.H. Rodrigues Pereira, M.T. Paulino Aguiar, P.R. Cetlin, Thermal stability of copper processed by multidirectional forging: Effect of deformation amplitude and cumulative strain. *Mater. Sci. Eng. A* **846**, 143299 (2022)
27. J. Tang, H. He, Y. Yi, S. Huang, H. Wang, J. Zhang, Effect of forging pretreatment on the microstructures and mechanical properties of the Al–Cu–Li alloy. *J. Alloys Compd.* **965**, 171379 (2023)
28. A. Sarkar, A. Bhowmik, S. Suwas, Microstructural characterization of ultrafine-grain interstitial-free steel by X-ray diffraction line profile analysis. *Appl. Phys. Mater. Sci. Process.* **94**(4), 943–948 (2009)
29. Q. Zhu, J. Wang, Y. Zuo, J. Cui, Effects of forging pass on the structure of 5182 aluminum alloy during multi-direction forging process. *J. Northeast. Univ. (Nat Sci).* **36**, 1572–1575 (2015)
30. W. Zhang, H. Lin, Y. Yi, S. Huang, Influence of thermomechanical processing on coarse particles, grain structure, and mechanical properties of Al–Cu alloy rings. *J. Mater. Res. Technol.* **22**, 1136–1150 (2023)
31. H. He, Y. Yi, S. Huang, Y. Zhang, Effects of cold pre-deformation on dissolution of second-phase Al₂Cu particles during solution treatment of 2219 Al–Cu alloy forgings. *Mater. Charact.* **135**, 18–24 (2018)
32. X. Zhang, J. Jiang, G. Li, X. Wang, W. Shao, L. Zhen, Particle-stimulated nucleation and recrystallization texture initiated by coarsened Al₂CuLi phase in Al–Cu–Li alloy. *J. Mater. Res. Technol.* **10**, 643–650 (2021)
33. Q. Yang, Y. Deng, M. Yang, Z. Zhang, W. Li, Q. Liu, Effect of Al₃Zr particles on hot-compression behavior and processing map for Al–Cu–Li based alloys at elevated temperatures. *Trans. Nonferrous Met. Soc. China* **30**, 870–882 (2020)
34. A.W. Zhu, E.A. Starke, Strengthening effect of unshearable particles of finite size: a computer experimental study. *Acta Mater.* **47**, 3263–3269 (1999)
35. L. Hu, M. Li, W. Huang, X. Yang, F. Guo, Compressive deformation behavior and microstructure evolution of AA2099 Al–Li alloy containing Al₃Li precipitates based on experimental characterization and crystal plasticity finite element simulation. *Mater. Sci. Eng. A* **852**, 143644 (2022)

Publisher's Note Springer Nature remains neutral with regard to jurisdictional claims in published maps and institutional affiliations.

Springer Nature or its licensor (e.g. a society or other partner) holds exclusive rights to this article under a publishing agreement with the author(s) or other rightsholder(s); author self-archiving of the accepted manuscript version of this article is solely governed by the terms of such publishing agreement and applicable law.